AN ABSTRACT OF THE THESIS OF

David C. Lund for the degree of Master of Science in Oceanography presented on October 30, 1997. Title: Millennial-scale Surface and Deep Water Oscillations in the N.E. Pacific: Implications for Late Pleistocene Climate Change

Abstract approved: Redacted for privacy

Alan C. Mix

Benthic foraminiferal stable isotopes and planktonic foraminiferal faunal assemblages are used to determine the character of millennial-scale climate change in the surface and deep (2700 m) Northeast Pacific (42°N, 126°W) from 10,000 to 60,000 years ago (10-60 ka). North Pacific Deep Water was better ventilated (high $\delta^{13}C$) during cold stadial conditions (high $\delta^{18}O$), opposite the pattern in the deep North Atlantic. Either the deep N.E. Pacific was ventilated from above, as a result of surface water cooling and increased salinity, or from below, through faster turnover of Pacific abyssal waters. During the Younger Dryas event (~11.6-12.8 ka), associated in the N. Atlantic with cooling and reduced deep water production, deep N.E. Pacific ventilation increased, but lagged that at intermediate depths (<450 m) by >500 years. This diachronous pattern suggests that low N. Atlantic turnover first affected the intermediate N.E. Pacific via atmospheric cooling and then the deep N.E. Pacific via thermohaline circulation. Foraminiferal-based modern analog sea-surface temperature estimates at 42°N, 126°W reveal a ~3°C cooling that lagged the Younger Dryas initiation by >500 years, implying atmospheric transmission alone did not cause N.E. Pacific temperature oscillations. Another mechanism must have been involved,

such as slow response of regional ice cover that modified atmospheric circulation over the N.E. Pacific, or, more likely, northward surface heat transport linked to deep water formation in the N. Pacific.

Millennial-scale Surface and Deep Water Oscillations in the N.E. Pacific: Implications for Late Pleistocene Climate Change

by

David C. Lund

A THESIS

submitted to

Oregon State University

in partial fulfillment of
the requirements for the
degree of

Master of Science

Completed October 30, 1997
Commencement June 1998

Master of Science thesis of David C. Lund presented on October 30, 1997

APPROVED:

Redacted for privacy

Major Professor, representing Oceanography

Redacted for privacy

Dean of the College of Oceanic and Atmospheric Sciences

Redacted for privacy

Dean of the Graduate School

I understand that my thesis will become part of the permanent collection of Oregon State University libraries. My signature below authorizes release of my thesis to any reader upon request.

Redacted for privacy

David C. Lund, Author

ACKNOWLEDGMENTS

I would like to thank my advisor, Alan Mix, for his support over the past three years. His guidance and advice were essential to this work. Ann Morey, Bill Rugh, June Wilson, and Candace Cloud were always helpful and in good spirits. In particular, I want to thank Ann for helping me identify all those bugs. I'd also like to thank my fellow paleo-students, Joe Ortiz, Sara Harris, Carolyn Viscosi-Shirley, Jim Watkins, and Leigh Welling. Working with them has been a pleasure. Sue Pullen, marine geology secretary extraordinaire, has helped me from start to finish, with everything from scheduling classes to sending off manuscripts. Thanks Sue.

I thank everyone in the COAS community who has made it an intellectually and socially stimulating place to be. I thank my friends in Corvallis for the sanity-saving mountain bike rides, ultimate games, and backyard barbecues. I thank my family for their support throughout the thesis process. Finally, I'd like to thank Kate Busse, for her friendship and moral support, and for feeding me the final few weeks before the defense. Without her, I would've eaten nothing but American Dream Pizza.

TABLE OF CONTENTS

TABLE OF CONTENTS (CONTINUED)

LIST OF FIGURES

Millennial-scale Surface and Deep Water Oscillations in the N.E. Pacific: Implications for Late Pleistocene Climate Change

1.

Introduction

The primary goals of this thesis have been (1) to determine if millennial-scale climate oscillations affected the deep N.E. Pacific, (2) to characterize sea-surface temperatures during the last deglaciation, and (3) to compare N.E. Pacific data to paleoclimate archives from the N. Atlantic region to evaluate potential climate change mechanisms. The results of this research are detailed in Chapters 2 and 3 of this thesis. Chapter 2 deals with benthic foraminiferal stable isotopic results spanning 10,000 to 60,000 years ago (10-60 ka). Chapter 3 considers the planktonic foraminiferal faunal assemblages during the last deglaciation (10-18 ka), focusing on the Younger Dryas cold interval (~11.6-12.8 ka). Chapter 4 includes a summary of primary results and potential directions for future work.

Recent paleoclimate research, particularly in the N. Atlantic region, has revealed that the ocean-atmosphere-cryosphere system is capable of changing much more rapidly than previously assumed. Surface temperatures in the N. Atlantic can switch from cold glacial-like (stadial) conditions, to warm interglacial-like (interstadial) conditions in a matter of decades (e.g. Dansgaard *et al.*, 1993). Each stadial or interstadial interval lasts for an average of one to two thousand years. Although the ultimate cause of millennial-scale climate oscillations is unknown, they appear to be linked to changes in Atlantic thermohaline circulation (e.g. Oppo and Lehman, 1995).

In Chapters 2 and 3 we present evidence for abrupt shifts in N.E. Pacific surface and deep water properties during the last glaciation. Our site (42°N, 126°W; 2700 m depth) is ideal for high-resolution paleoceanographic reconstructions because it monitors North Pacific Deep Water, but it is

shallow enough to allow for calcite preservation. Proximity to N. America (and hence input of terrigenous clays) provides the sedimentation rate necessary to capture millennial-scale climate change.

Benthic foraminiferal $\delta^{18}O$ and $\delta^{13}C$ are compared to a sea-surface temperature (SST) record from the N. Atlantic and to a record of intermediate water ventilation from the Santa Barbara Basin (Chapter 2). Planktonic foraminiferal assemblages are used to estimate SST in the N.E. Pacific, and results are compared to the Younger Dryas cold interval in Greenland ice cores (Chapter 3). The relative timing of events at each site is used to assess potential teleconnection pathways between the Atlantic and Pacific during the Late Pleistocene. Synchronous change in the two basins would imply linkage via the atmosphere, whereas a time lag would implicate slower responding components of the climate system, such as the cryosphere or deep ocean circulation.

2.

Millennial-scale Deep Water Oscillations: Reflections of the North Atlantic in the Deep Pacific from 10 to 60 ka

David C. Lund and Alan C. Mix

Submitted to *Paleoceanography*,
American Geophysical Union, Washington D.C.
May 1997, 34 pages, in press.

2.1 ABSTRACT

Northeast Pacific benthic foraminiferal $\delta^{18}O$ and $\delta^{13}C$ reveal repeated millennial-scale events of strong ventilation (nutrient depletion and/or gas exchange) during stadial (cool, high ice volume) episodes from 10 to 60 ka, opposite the pattern in the deep N. Atlantic. Two climate mechanisms may explain this pattern. North Pacific surface waters, chilled by atmospheric transmission from a cold N. Atlantic and made saltier by reduced fresh-water vapor transports, may have ventilated the deep Pacific from above. Alternatively, faster turnover of Pacific bottom and mid-depth waters, driven by Southern Ocean winds, may have compensated for suppressed North Atlantic Deep Water production during stadial intervals. During the Younger Dryas event (~11.6-12.8 cal ka), ventilation of the deep N.E. Pacific (~2700 m) lagged that in the Santa Barbara Basin (~450 m) by >500 y, suggesting that the N.E. Pacific was first ventilated at intermediate depths from above and then at greater depth from below. This apparent lag may reflect the adjustment time of global thermohaline circulation.

2.2 INTRODUCTION

Evidence for millennial-scale climatic shifts is beginning to emerge on a global basis [e.g. Grimm *et al.*, 1993; Behl and Kennett, 1996; Bard *et al.*, 1997]. These fluctuations appear to be related to changes in North Atlantic Deep Water (NADW) formation rate [e.g., Oppo and Lehman, 1995], but the behavior of abyssal waters in other ocean basins has remained a mystery. Here we present evidence for millennial-scale oscillations in North Pacific

Deep Water (NPDW) composition from 10 to 60 ka. The pacing of NPDW change is similar to climatic cycles observed in the North Atlantic. Unlike the Atlantic, however, ventilation in the Pacific generally increases during cold (i.e., stadial) intervals. We offer two possible explanations for this phenomenon, one which involves deep water formation in the North Pacific, and the other which calls upon enhanced Pacific mid-depth outflow to compensate deep upwelling near Antarctica. Both are tied to Atlantic thermohaline overturn and therefore represent potential mechanisms for propagating millennial-scale climate events around the globe.

Most of the early evidence for abrupt glacial climate change comes from the North Atlantic region. Oxygen isotope ratios in Greenland ice cores outline 2-3 kyr warm-cold oscillations, known as Dansgaard-Oeschger temperature cycles [Dansgaard *et al.*, 1993; Grootes *et al.*, 1993]. Similar patterns exist in the temperature-sensitive coiling ratio of the planktonic foraminifer *Neogloboquadrina pachyderma* from North Atlantic sediments [Lehman and Keigwin, 1992; Bond *et al.*, 1993; Oppo and Lehman, 1995]. Layers of ice-rafted detritus in these sediments imply that increased iceberg flux occurred near the end of each stadial period [Bond and Lotti, 1995]. Groups of stadial intervals fall into longer-term (7-10 kyr) cooling cycles, themselves punctuated by massive "Heinrich" ice rafting events [Bond *et al.*, 1993].

North Atlantic Deep Water properties shifted with millennial-scale climatic oscillations. Benthic foraminiferal $\delta^{13}C$ from the subpolar North Atlantic suggests that low sea-surface temperatures (SSTs) during the last glacial period were generally associated with reduced Atlantic thermohaline

circulation [Oppo and Lehman, 1995]. Carbonate records from the mid-latitude Atlantic indicate similar shifts in NADW production [Keigwin and Jones, 1994]. Consistent with this pattern, millennial-scale SST lows in the equatorial Atlantic (planktonic foraminiferal $\delta^{18}O$ highs) match apparent decreases in NADW (benthic foraminiferal $\delta^{13}C$ lows) [Curry and Oppo, 1997].

Geologic records from shallow marginal basins of the Northeast Pacific indicate that millennial-scale climate change extended beyond the North Atlantic region. In the Santa Barbara Basin (sill depth 450 m), laminated intervals, benthic and planktonic foraminiferal $\delta^{18}O$, and the coiling ratio of *N. pachyderma* show that surface water cooling and enhanced basin ventilation occurred near the time of the N. Atlantic Younger Dryas cool event [Kennett and Ingram, 1995]. Laminations in the Gulf of California [Keigwin and Jones, 1990] contemporary with those in the Santa Barbara Basin imply a regional switching from oxygen-poor to oxygen-rich conditions at intermediate water depth (< 700 m) [Kennett and Ingram, 1995]. Behl and Kennett [1996] suggest that laminated intervals in the Santa Barbara Basin correlate with interstadial events in Greenland over the past 60,000 years, hinting at a connection between the processes which control surface temperatures in the North Atlantic and intermediate water composition in the Northeast Pacific. The mechanism by which the Atlantic and Pacific were connected remains ambiguous.

2.3 MODERN OCEANOGRAPHIC SETTING

Due to the large salinity-driven density contrast between surface and underlying waters, there is little or no deep water formation in the modern North Pacific [Warren, 1983]. Rather, Pacific Bottom Water (PBW) is a blend of ~70% southern (Antarctic) component, ~15% northern (NADW) component, and ~15% intermediate component water [Broecker *et al.*, 1985]. The intermediate component is a composite of Antarctic intermediate waters (<1 km depth) which have mixed with overlying water in the Pacific and Indian oceans. Further mixing of the intermediate component with bottom waters (>4 km depth) in the Pacific and Indian basins composes mid-depth (2-3 km) outflow to the Antarctic. This outflow then combines with the southern and northern components to produce the so-called "Common Water". Mixing of "Common Water" with the southern component creates PBW [Broecker *et al.*, 1985].

Moving from the southwest to northeast Pacific, PBW generally becomes warmer and less saline, less oxygenated, and higher in dissolved silicate content [Mantyla and Reid, 1983]. North Pacific Deep Water (NPDW) is apparently created in the Northeast Pacific Basin, through exposure of PBW to geothermal heat and cross-isopycnal mixing with overlying warmer, less saline water [Mantyla, 1975]. NPDW spreads southward as a mid-depth return flow, separated from the northward flowing PBW by a stability maximum near 4 km depth [Mantyla, 1975]. The core of the return flow is at 2-3 km depth, below the effective sill depth at Drake Passage, a key geostrophic constraint on southward advection in the ocean's interior (Toggweiler and Samuels, 1995).

2.4 METHODS & MATERIALS

The sediment core used for this study, W8709A-13PC (2712 m depth; 42.1 °N, 125.8 °W), comes from the eastern flank of the Gorda Ridge and is predominantly composed of hemipelagic clay, with low (<15%) carbonate and opal content. Today, the site is bathed in North Pacific Deep Water (NPDW) and is below the regional carbonate compensation depth of 2400 m [Lyle *et al.*, 1992]. From approximately 10 to at least 45 ka, however, the CCD was generally deeper than 2700 m [Karlin *et al.*, 1992]. There are five small sandy silt layers (inferred to be distal turbidites) in W8709A-13PC, at 206-208 cm, 230-232 cm, 252-256 cm, 322-325 cm, and 355-358 cm.

2.4.1 Stable Isotopes

Isotope samples were taken at 3 cm intervals from 99-761 cm and 20 cm intervals from 40-99 cm and 761-868 cm. We separated three species of benthic foraminifera from the >150 μm fraction, *Cibicidoides wuellerstorfi*, *Uvigerina senticosa*, and *Uvigerina peregrina*. On average there were six *C. wuellerstorfi* individuals per analysis. For *Uvigerina spp.* the average was seven. The microfossils were cleaned ultrasonically in alcohol, dried, and then roasted for 1 hour at 400°C under high vacuum. All isotope measurements were made at Oregon State University using a Finnigan-MAT251 coupled to an Autoprep Systems carbonate device. Reactions occurred under vacuum in ~100% orthophosphoric acid at 90°C.

Analytical precision of the local standard (a pure fine-ground calcitic marble) over the same period as the foraminiferal analyses was 0.05‰ for $\delta^{18}O$ and 0.02‰ for $\delta^{13}C$ ($\pm 1\ \sigma$, n = 328). Primary calibration to the PDB standard was through NBS-20, supplied by the U.S. National Institute for Standards and Technology, assuming NBS-20 $\delta^{18}O$ = -4.14‰ and $\delta^{13}C$ = -1.06‰ (supported by analyses of NBS-19). Precision of NBS-20 was 0.06‰ for $\delta^{18}O$ and 0.02‰ for $\delta^{13}C$ ($\pm 1\ \sigma$, n = 14).

2.4.2 Chronostratigraphy

The age model for W8709A-13PC was constructed using 21 calendar-corrected ^{14}C ages, the marine oxygen isotope stage 3-4 boundary at 59 ka [Imbrie *et al.*, 1984], and 5 ages from North Atlantic core V23-81 (Figure 2.1a). Radiocarbon control for W8709A-13PC spans 7 to 36 ka. Dates original to this paper are based on planktonic foraminifera run at Lawrence Livermore National Laboratory (Table 1). AMS dates from Gardner *et al.* [1997] are based on 5 mg samples of mixed planktonic and mixed benthic foraminifera and those from Lyle *et al.* [1992] are based on 5-10 mg samples of mixed planktonic foraminifera.

Reservoir-corrected ages were calculated by subtracting 718 and 2380 years from the raw planktonic and benthic ^{14}C ages, respectively [Ortiz *et al.*, 1997]. At depths where both benthic and planktonic reservoir-corrected values were determined, we used the average.

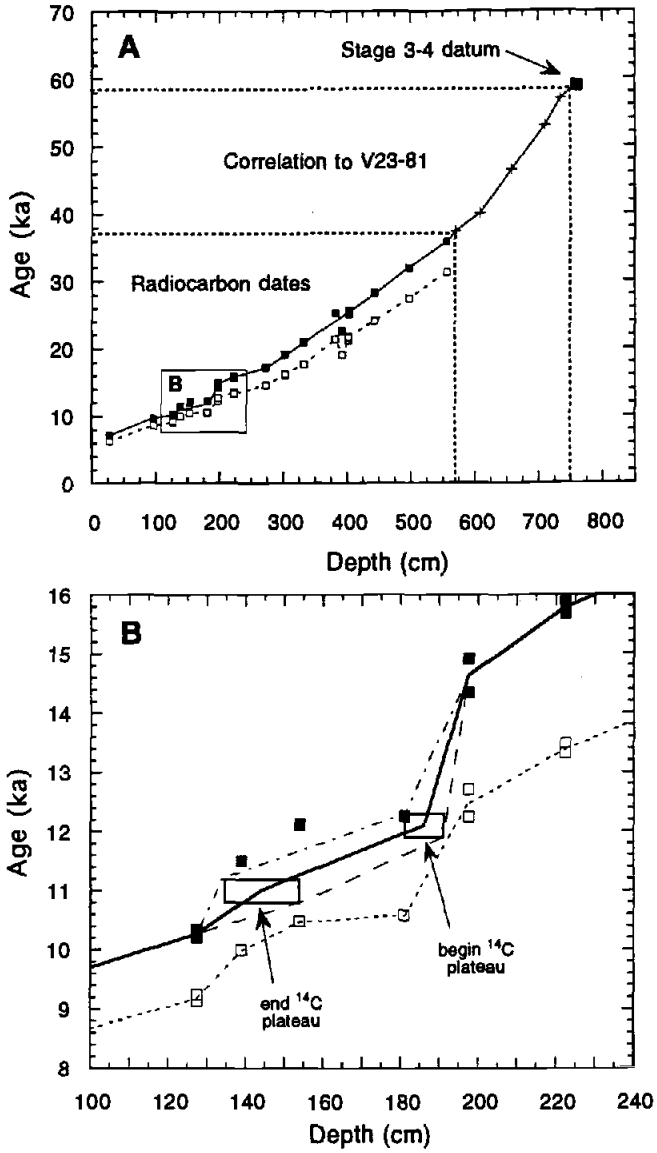

Figure 2.1 Age model for W8709A-13PC. A) Reservoir-corrected radiocarbon dates are represented with open squares and corresponding calendar ages with solid squares. Dates from 36-57 kyr BP are based on correlation of millennial-scale $\delta^{18}O$ highs to stadial intervals in North Atlantic core V23-81. The datum at 59 kyr BP marks the marine isotope stage 3-4 boundary in W8709A-13PC. All dates are listed in Table 1. B) Age model options for the interval between 130 and 195 cm. We use reservoir-corrected dates in this interval to define the stratigraphic position of the ^{14}C plateau and then apply known ages for the beginning and end of the plateau to the appropriate depths (see text). The oldest possible age model is between the upper left-hand corner of each box, and the youngest possible age model is between the lower right-hand corners. The age model used in this paper is an average of these two end-members (solid line).

Depth (cm)	Raw AMS age (ka)	Raw error (ka)	Reservoir-corrected age (ka)	Calendar Age (ka)	Inferred Calendar Age (ka)	Species and sample weight (if available)	Source
27.5	7.00	0.23	6.28	7.18	–	mixed planktonic	A
97.5	11.01	0.36	8.63	9.64	–	mixed benthic	A
127.5	11.51	0.33	9.14	10.27	–	mixed benthic	A
127.5	9.96	0.23	9.24	–	–	mixed planktonic	A
139	10.72	0.07	10.00	11.50	10.8	*N. pachyderma* & *G. bulloides* (3.5 mg)	B
154	11.20	0.06	10.48	12.12	11.3	*N. pachyderma* (5.6 mg)	B
181	11.31	0.14	10.59	12.26	12.0	*N. pachyderma* (6.1 mg)	B
197.5	14.63	0.39	12.25	14.63	–	mixed benthic	A
197.5	13.43	0.19	12.71	–	–	mixed planktonic	A
222.5	15.86	0.50	13.48	15.77	–	mixed benthic	A
222.5	14.04	0.28	13.32	–	–	mixed planktonic	A
272.5	15.27	0.22	14.55	17.18	–	mixed planktonic	C
302.5	18.49	0.38	16.12	19.10	–	mixed benthic	A
302.5	16.87	0.27	16.15	–	–	mixed planktonic	A
332.5	18.37	0.27	17.65	20.90	–	mixed planktonic	C
382	22.14	0.14	21.42	25.28	–	*G. bulloides* (10.6 mg)	B
392.5	19.82	0.61	19.10	22.61	–	mixed planktonic	C
402.5	24.05	1.53	21.67	25.32	–	mixed benthic	A
402.5	21.96	0.49	21.24	–	–	mixed planktonic	A
443	24.78	0.14	24.06	28.25	–	*G. bulloides* (9.8 mg)	B
497	28.14	0.40	27.42	31.91	–	*G. bulloides* (12.1 mg)	B
557	31.97	0.32	31.25	35.92	–	*G. bulloides* (11.7 mg)	B

Depth (cm)	Calendar Age (ka)	Method:
570	37.4	Correlation of $\delta^{18}O$ maximum to stadial interval in North Atlantic core V23-81.
608	40.0	"
658	46.5	"
710	53.0	"
735	57.0	"
760	59.0	Marine oxygen isotope stage 3-4 transition in W8709A-13PC.

Table 1 Ages for W8709A-13PC used in this study, including raw AMS age, analytical error, corresponding reservoir-corrected and calendar age, foraminiferal species type and sample weight (in mg $CaCO_3$). Depths for ^{14}C dates written in whole numbers are ±1 cm, all other AMS depths are ±2.5 cm. Also included are ages inferred from the "average" age model in Figure 2.1b, ages determined by correlation of $\delta^{18}O$ maxima to stadial intervals in North Atlantic core V23-81, and the marine oxygen isotope stage 3-4 boundary in W8709A-13PC. Source A, Gardner *et al.* [1997]; source B, this study; source C, Lyle *et al.* [1992].

Radiocarbon dates younger than 10,500 reservoir-corrected years were converted to calendar ages following Stuvier and Braziunas [1993]. In this calibration, calendar ages are calculated as:

$$\text{Calendar age (years)} = R_m - (R_t + \Delta R)$$

where R_m is the measured ($\delta^{13}C$ corrected) radiocarbon age, R_t is a time-dependent simulation of the global surface ocean which includes a nominal 400 year reservoir correction, and ΔR is an additional regional shift in the reservoir age that is assumed, as a first approximation, to be constant. We used a ΔR value of 320 years and 1980 years for the planktonic and benthic raw ^{14}C ages, respectively.

Reservoir-corrected ages in W8709A-13PC older than 10,500 radiocarbon years were transformed to calendar years using the equation of Bard *et al.* [1992]:

$$\text{Calendar age, in years} = -5.85\text{x}10^{-6} * (A^2)+(1.39*A)-1807$$

where A is reservoir-corrected radiocarbon age in years. This equation is calibrated from 10,000 to 38,000 radiocarbon years, but corrections older than 22,000 years are not well constrained [Bard *et al.*, 1992]. The calendar ages from 382 to 403 cm were averaged to produce one age.

Ages from 36 to 57 ka are based on correlation of millennial-scale $\delta^{18}O$ peaks in W8709A-13PC to stadial intervals in North Atlantic core V23-81 [Bond *et al.*, 1993]. We converted the reservoir-corrected ^{14}C age model for V23-81 [Bond *et al.*, 1993] to calendar years using the Bard *et al.* [1992]

equation. Ages for samples between the dated control points were calculated by linear interpolation.

A zone of nearly constant ^{14}C dates is apparent in W8709A-13PC at 10,000 ^{14}C years (Figure 2.1b), which we infer as the deglacial radiocarbon "plateau" [Stuiver and Braziunas, 1993; Edwards *et al.*, 1993]. Using standard calendar correction formulas in this zone produces ambiguous results, because the formulas can't distinguish between the top and bottom of the plateau. Rather than use these ages directly, we used them to define the stratigraphic position of constant ^{14}C in W8709A-13PC. We then applied known calendar ages for the beginning (11.9-12.3 ka) and end (10.8-11.2 ka) of the plateau [Stuiver and Braziunas, 1993; Edwards *et al.*, 1993] to the ^{14}C-constrained depths for the beginning (181-191 cm) and end (134-154 cm) of the plateau. Possible depth vs. time positions for the plateau are outlined with rectangular boxes in Figure 2.1b. The youngest possible age model is defined by the lower right-hand corner of each box and the oldest possible age model is defined by the upper left-hand corners. The age model used here is the average of these two end-members, applied to 138, 154, and 181 cm (Table 1).

2.5 RESULTS

2.5.1 Glacial-interglacial Changes

On glacial-interglacial time scales, high values of $\delta^{18}O$ correspond to low (more negative) values of $\delta^{13}C$ in W8709A-13PC (Figure 2.2). During

marine oxygen isotope stages 2 and 4, ^{18}O is enriched by as much as 1.5‰ relative to the early Holocene. In Figure 2, *Uvigerina spp.* $\delta^{18}O$ is used for the upper 110 cm of the core, due to a lack of *C. wuellerstorfi* in this interval.

C. wuellerstorfi $\delta^{13}C$ is low during stages 2 and 4, with values typically between -0.5‰ to -0.6‰, about 0.3‰ lower than in stage 1. This 0.3‰ offset is similar to the global glacial-interglacial average [Curry *et al.*, 1988] and the pattern is consistent with that attributed to fluctuations in terrestrial biomass [Shackleton, 1977]. In stage 3, $\delta^{13}C$ reaches -0.2 per mil in some intervals, close to modern $\delta^{13}C$ values for total dissolved inorganic carbon (ΣCO_2) in the deep Northeast Pacific [Kroopnick, 1985].

2.5.2 Millennial-scale Oscillations

Both $\delta^{18}O$ and $\delta^{13}C$ display millennial-scale (< 10 kyr period) variability during marine oxygen isotope stages 2 and 3. Positive $\delta^{18}O$ excursions (values 0.1-0.3 per mil higher than adjacent intervals) occur repeatedly, with the most variability concentrated in stage 3. Millennial-scale peaks in $\delta^{13}C$ of 0.1 to 0.3 per mil tend to occur during intervals of high $\delta^{18}O$, opposite the glacial-interglacial pattern, but there are exceptions. For example, $\delta^{13}C$ lows near 290, 410, 500, 570 and 615 cm interrupt positive $\delta^{13}C$ excursions, producing double $\delta^{13}C$ peaks. Also, there is no discernible $\delta^{18}O$ high accompanying the $\delta^{13}C$ peaks at 170 and 525 cm and the positive $\delta^{18}O$ excursion near 740 cm has no corresponding change in $\delta^{13}C$. In general, it appears that $\delta^{13}C$ is more variable during $\delta^{18}O$ highs than lows.

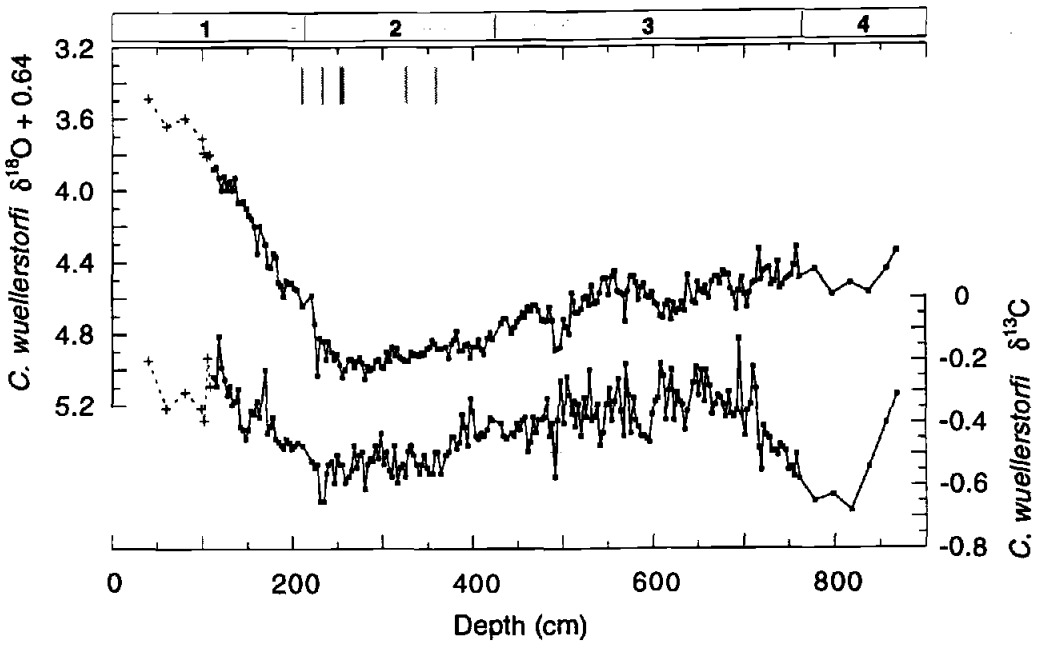

Figure 2.2 *C. wuellerstorfi* $\delta^{18}O$ and $\delta^{13}C$ vs. depth in W8709A-13PC. Samples above 110 cm are *Uvigerina spp.* (*U. senticosa* and *U. peregrina*) (pluses). *C. wuellerstorfi* $\delta^{18}O$ values (squares) were adjusted by +0.64‰ to match the *Uvigerina* scale. Marine oxygen isotope stages 1-4 are indicated on the upper x-axis. On Milankovitch time-scales $\delta^{18}O$ and $\delta^{13}C$ are inversely correlated while on millennial time-scales $\delta^{13}C$ maxima generally occur during $\delta^{18}O$ maxima. Small sandy silt layers (apparently turbidites) at 206-208 cm, 230-232 cm, 252-256 cm, 322-325 cm, and 355-358 cm are marked with gray rectangles. Stable isotopic data are listed in Appendix A.

2.6 DISCUSSION

2.6.1 Timing of Events

From 10 to 60 ka, $\delta^{18}O$ and $\delta^{13}C$ maxima occurred every 4-6 kyr on average, similar to the pacing of millennial-scale polar front advances in the North Atlantic (Figure 2.3). Direct comparison of the benthic isotope record in W8709A-13PC with %*N. pachyderma (s.)* in core V23-81 suggests that each $\delta^{18}O$ high in the N.E. Pacific has a corresponding sea-surface temperature low in the N. Atlantic. $\delta^{18}O$ maxima centered near 17, 25, 32, 41, and 50 ka align with the stadial intervals terminated by Heinrich events 1, 2, 3, 4, and 5, respectively. $\delta^{18}O$ peaks near 37, 46 and 57 ka also correspond to high %*N. pachyderma (s.)* in core V23-81. There is a small $\delta^{18}O$ maximum (<0.1‰) near the time of the Younger Dryas, interrupting the glacial-interglacial transition.

Some of the Dansgaard-Oeschger temperature cycles apparent in the GRIP ice core from Greenland [Dansgaard *et al.*, 1993] are absent from the N.E. Pacific $\delta^{18}O$ and N. Atlantic SST records (see Bond *et al.* [1993] for comparison of V23-81 and GRIP). For example, in the time interval between Heinrich events 3 and 4, there are four apparent interstadial events in GRIP, two in V23-81 and two $\delta^{18}O$ lows in W8709A-13PC. This may be a function of bioturbation in the sedimentary records and the higher sampling resolution for the GRIP core. Between 10 and 60 ka, samples in W8709A-13PC were taken every 250 years on average, in V23-81 every 200 years [Bond *et al.*, 1993], and in GRIP every 130 years [Dansgaard *et al.*, 1993].

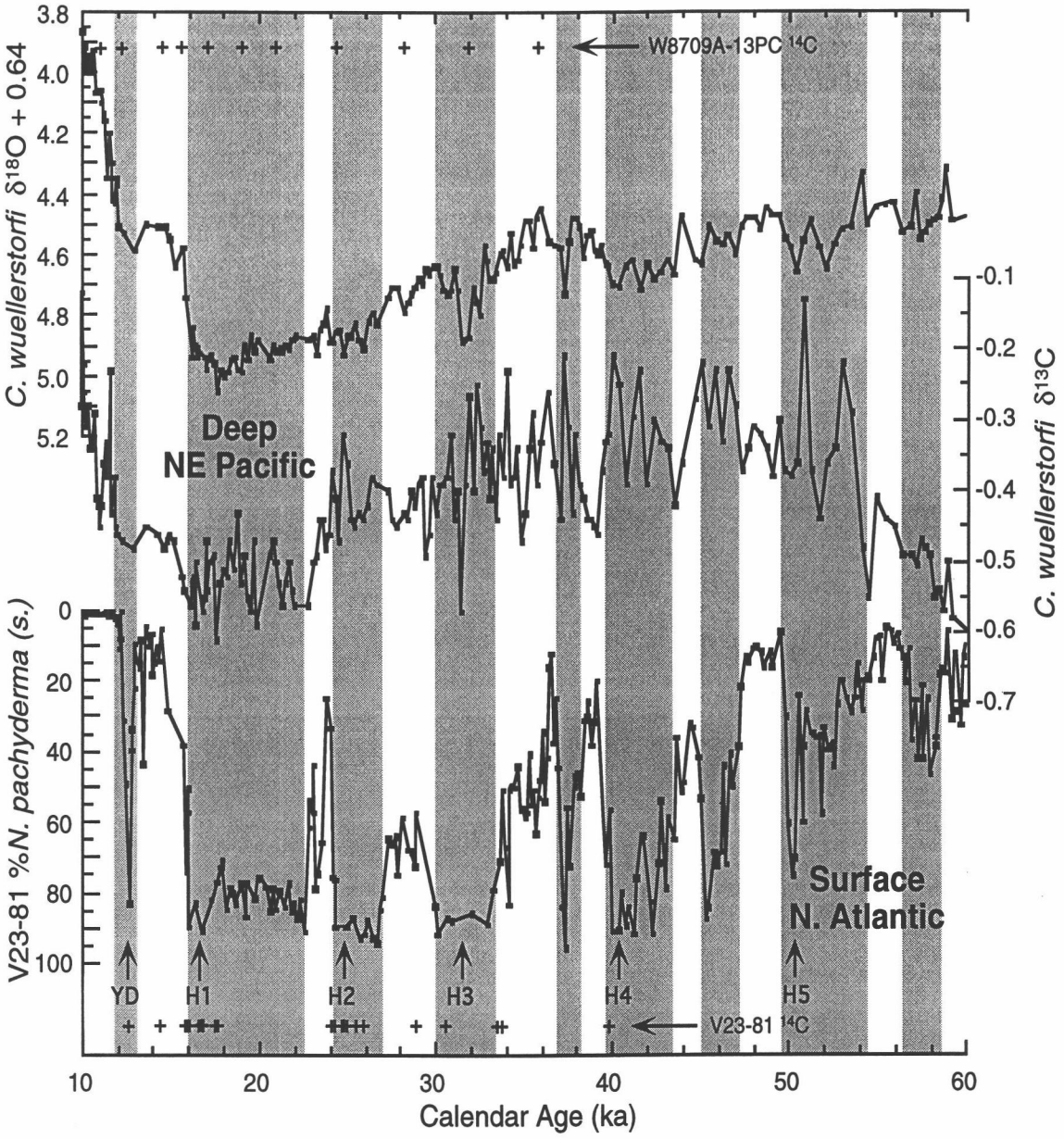

Figure 2.3 *C. wuellerstorfi* $\delta^{18}O$ and $\delta^{13}C$ in W8709A-13PC and *%N. pachyderma (s.)* in North Atlantic core V23-81 plotted vs. calendar age. Shaded areas represent cold (stadial) intervals in the N. Atlantic. Millennial-scale $\delta^{18}O$ and $\delta^{13}C$ maxima generally correspond to stadial conditions and ^{18}O depletions tend to occur near the time of ice-rafting events. Ages for Heinrich ice-rafting events from Bond et al. [1993] are in calendar years. Calendar-corrected radiocarbon dates for W8709A-13PC (+) are marked on the upper x-axis and those for V23-81 (+) are marked on the lower x-axis. Samples near turbidites in which sand grains composed >50% of the >150 μm particles were excluded from Figure 2.3. This includes samples at 227, 230, 234, 252, 255, 258, 319, 322, 325, 355, 358, and 361 cm in W8709A-13PC. Isotope values at these depths are shown in Figure 2.2.

Positive $\delta^{13}C$ excursions in W8709A-13PC generally occur during stadial conditions. $\delta^{13}C$ peaks at 24.5, 26, 31, 33, 37, 40, 46, 51, and 53 ka each correspond to low SST in the North Atlantic (Figure 2.3). The correlation between $\delta^{13}C$ and SST is less consistent than for $\delta^{18}O$, however. For example, relatively low $\delta^{13}C$ at 25 and 32 ka occur during stadial conditions. The processes controlling deep Pacific $\delta^{13}C$ seem particularly sensitive during intervals of extreme cold in the N. Atlantic.

Ages for isotopic events younger than 36 ka are well constrained by radiocarbon dating. Ages from 37 to 59 ka were tuned by correlation of $\delta^{18}O$ maxima in W8709A-13PC to V23-81 stadial intervals. Therefore, in this interval, the correlation between the two records should be considered tentative. During cold episodes, however, it is likely that either (1) global ice volume increased, or (2) deep waters became cooler. In either case, $\delta^{18}O$ would become heavier, consistent with our method of matching $\delta^{18}O$ maxima to stadial intervals. Also, older isotopic events are similar to those in the interval constrained by radiocarbon dating, both in signal amplitude and period, and dates determined by correlation of $\delta^{18}O$ maxima to V23-81 stadial intervals align well with ^{14}C ages and the marine oxygen isotope stage 3-4 boundary in W8709A-13PC (Figure 2.1a).

Shifting ventilation patterns could potentially affect reservoir ages in the N.E. Pacific. Southon *et al.* [1990] calculated a N.E. Pacific surface water reservoir age of 1200 years at 6,400 ^{14}C years BP, nearly 500 years older than the correction used in this paper. Altering the correlation of $\delta^{18}O$ maxima to N. Atlantic stadial conditions, however, would require reservoir age fluctuations on the order of 2 kyr (Figure 2.3). Benthic ^{14}C ages were

corrected using a reservoir age of 2380 years. Although this too may have changed through time, five of the six benthic foraminiferal dates in W8709A-13PC were cross-checked with a planktonic date in the same sample, with an average difference of less than 250 years [Ortiz *et al.*, 1997]. Since ~2 kyr changes in reservoir age are highly unlikely, we infer that glacial millennial-scale isotopic enrichments in the N.E. Pacific were contemporary with extreme cooling in the North Atlantic.

2.6.2 Oxygen Isotopes

Benthic foraminiferal $\delta^{18}O$ is subject to both temperature and ice volume effects. If the ~0.2‰ $\delta^{18}O$ excursions in W8709A-13PC were entirely due to temperature, this would require deep water temperature oscillations of approximately 1°C (assuming a thermodynamic relationship of 0.22 per mil/°C; Epstein *et al.* [1953]). Is this reasonable? Deep Pacific temperatures during oxygen isotope stages 2 and 3 were about 2°C lower than at present, based on comparison of benthic foraminiferal $\delta^{18}O$ in core V19-30 from the equatorial Pacific and sea level estimates from coral terraces in New Guinea [Chappell and Shackleton, 1986; Chappell *et al.*, 1996]. Today, potential temperature is ~1.5°C in the vicinity of W8709A-13PC and V19-30 [Broecker *et al.*, 1982]. Similar glacial $\delta^{18}O$ values at the two sites [Shackleton *et al.*, 1983] implies that glacial deep water temperature at each location was near -0.5°C. Since the coral terraces formed mostly during sea level high stands (low ice volume, depleted oceanic $\delta^{18}O$), millennial-scale ^{18}O enrichments in W8709A-13PC, if due to temperature alone, would suggest cooling to -1.5°C, close to the freezing point of sea water (-1.9°C). Results from a simple box

model imply that this would require an unrealistic increase in deep water turnover rates [Mix and Pisias, 1988].

Alternatively, fluctuations in global ice volume could have influenced N.E. Pacific $\delta^{18}O$. A ~0.2 per mil $\delta^{18}O$ oscillation is equivalent to about 20 m of sea level change [Fairbanks, 1990; Chappell and Shackleton, 1986]. Stage 3 sea level fluctuations of 20-30 m have been observed in coral terraces of New Guinea [Chappell *et al.*, 1996]. Also, several $\delta^{18}O$ maxima in W8709A-13PC end near the time of ice rafting events, when massive quantities of ^{18}O-depleted ice discharged into the North Atlantic (Figure 2.3). Thus, although temperature may account for a portion of each ~0.2 per mil oscillation, the timing and magnitude of $\delta^{18}O$ shifts in the N.E. Pacific points to ice volume as a more probable explanation.

2.6.3 Carbon Isotopes

Oscillations in benthic $\delta^{13}C$ can be caused by changes in terrestrial biomass, organic carbon input from surface waters, air-sea gas exchange, and water mass composition. On millennial time scales, peaks in $\delta^{13}C$ generally occur during positive $\delta^{18}O$ excursions, inconsistent with the glacial-interglacial pattern in which low $\delta^{13}C$ is associated with high $\delta^{18}O$. Results from the North Atlantic show that benthic $\delta^{13}C$ was generally depleted during stadial intervals of the last 60 ka [Oppo and Lehman, 1995], opposite the pattern the N.E. Pacific. Given these temporal and regional differences, it seems unlikely that changes in terrestrial biomass caused the short-term $\delta^{13}C$ fluctuations in W8709A-13PC.

Although *Cibicidoides spp.* are generally considered the most reliable foraminiferal recorders of deep water $\delta^{13}C$ [Curry *et al.*, 1988], the $\delta^{13}C$ signal may be complicated by organic carbon input to the surface sediments. For example, in the modern Antarctic, *Cibicidoides spp.* are sometimes depleted in $\delta^{13}C$ relative to bottom waters, probably as a result of epibenthic decay of $\delta^{13}C$-depleted organic matter [Mackensen *et al.*, 1994]. To determine whether the so-called "Mackensen effect" altered the signal in W8709A-13PC, we plotted *C. wuellerstorfi* $\delta^{13}C$ versus the difference in *C. wuellerstorfi* and *Uvigerina spp.* $\delta^{13}C$ ($\Delta\delta^{13}C$), measured in the same samples (Figure 2.4). Since *Uvigerina spp.* have an infaunal habitat [Zahn *et al.*, 1986], and *C. wuellerstorfi* an epifaunal one [Corliss, 1985], higher organic carbon flux should result in enhanced $\Delta\delta^{13}C$ [Zahn *et al.*, 1986]. Figure 2.4 shows that *C. wuellerstorfi* $\delta^{13}C$ has a weak positive correlation with $\Delta\delta^{13}C$ (r=0.54), opposite the trend expected if the "Mackensen effect" drove local $\delta^{13}C$ variations. Therefore, it appears that pore water effects have not significantly altered *C. wuellerstorfi* $\delta^{13}C$.

The $\delta^{13}C$ of deep water, and hence benthic foraminifera, can also be altered through surface ocean CO_2 exchange with the atmosphere. At isotopic equilibrium, colder water has higher $\delta^{13}C$ and warmer water has lower $\delta^{13}C$ [Broecker and Maier-Reimer, 1992]. This thermodynamic effect ($\delta^{13}C_{as}$, for air-sea exchange) is independent of nutrient-related changes in $\delta^{13}C$. Glacial maximum reconstructions suggest that deep northwest Pacific $\delta^{13}C_{as}$ was up to ~0.7‰ higher than at present [Lynch-Stieglitz and Fairbanks, 1994]. If gas exchange effects were this large in the Pacific, the ~0.2‰ millennial-scale $\delta^{13}C$ oscillations in W8709A-13PC could be related to the extent of air-sea equilibration in N. Pacific source waters. With $\delta^{13}C$ data

alone it would be difficult to distinguish between greater gas exchange and lower nutrients, but both imply greater ventilation during cold events.

The simplest, and we think most likely, explanation for the ^{13}C enrichments in W8709A-13PC is that NPDW was influenced by a ^{13}C-enriched water mass during these episodes or the residence time of Pacific deep and bottom waters decreased. Enrichment of ^{13}C could have occurred through mixing with a "new" deep water source proximal to the N.E. Pacific with high preformed $\delta^{13}C$ (> -0.2 per mil), or through colder equilibration temperatures (higher $\delta^{13}C_{as}$) at deep-water sources which feed the Pacific. A glacial deep water source in the Pacific has been proposed by Curry *et al.* [1988] to reconcile higher mean $\delta^{13}C$ in the Pacific relative to the Southern Ocean during the Last Glacial Maximum, Ohkouchi *et al.* [1994] to explain low LGM Cd/Ca in the deep northwest Pacific, and Lynch-Stieglitz and Fairbanks [1994] to account for global $\delta^{13}C_{as}$ patterns during the last glaciation.

Fluctuations in residence time of Pacific Bottom Water could also account for the ~0.2 per mil $\delta^{13}C$ peaks noted in W8709A-13PC. The longer a water mass resides in the deep sea, the more organic material degrades within it, consuming oxygen and depleting ^{13}C. In the modern ocean, water mass "aging" accounts for the 0.4 per mil depletion of PBW $\delta^{13}C$ relative to southern component waters [Curry *et al.*, 1988]. Increasing the turnover rates of deep and bottom waters in the N. Pacific should decrease residence time and thus enrich local ^{13}C. Deep water changes may have occurred sporadically during each heavy $\delta^{18}O$ interval, since $\delta^{13}C$ is more variable during these times.

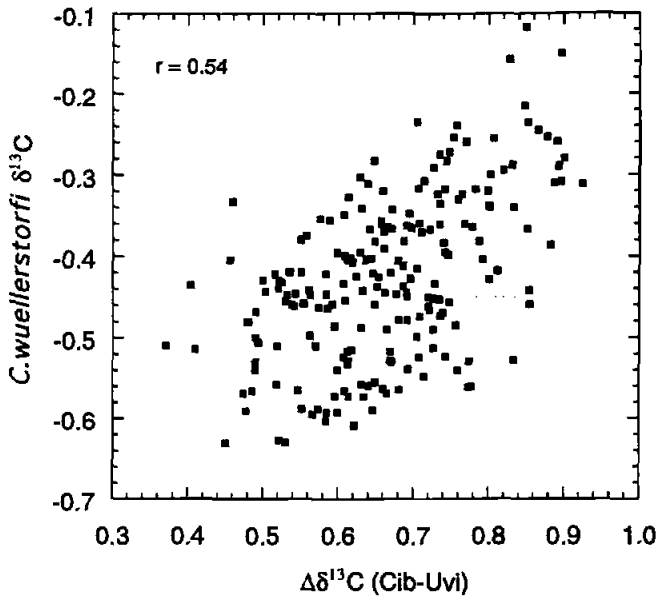

Figure 2.4 $\Delta\delta^{13}C$ (*C. wuellerstorfi* $\delta^{13}C$ - *Uvigerina spp.* $\delta^{13}C$) vs. *C. wuellerstorfi* $\delta^{13}C$. During intervals of enhanced organic carbon delivery, $\Delta\delta^{13}C$ should increase. If the 'Mackensen effect' drove *C. wuellerstorfi* $\delta^{13}C$, $\Delta\delta^{13}C$ and *C. wuellerstorfi* $\delta^{13}C$ would be negatively correlated. Instead, there is a weak positive correlation (r = 0.54).

2.6.4 Ventilation from Above

In the modern ocean, deep water forms in the North Atlantic but not in the North Pacific. The primary reason for this contrast is the precipitation-evaporation patterns in the two basins. In the North Pacific, precipitation greatly exceeds evaporation, whereas in the North Atlantic they are nearly balanced [Baumgartner and Reichel, 1975]. Low evaporation in the North Pacific causes a large surface to deep density contrast, limiting the sinking of surface water to intermediate depths [Warren, 1983].

The tendency for intermediate-depth ventilation to occur in the northwest Pacific [Reid, 1965; Talley, 1991; 1993] highlights this region as a candidate for deep water formation during glacial times. A similar potential exists in the Bering Sea, where the presence of chlorofluorocarbons in bottom waters implies that some (~1 Sv) deep water production may occur there today [Warner and Roden, 1995]. The N.E. Pacific seems an unlikely candidate, since the upper water column there was apparently more stable at the Last Glacial Maximum than today [Zahn *et al.*, 1991].

If deep water formed in the North Pacific during stadial intervals, the density contrast between surface and deep waters must have decreased relative to the modern ocean. One way to do this would be to change the precipitation-evaporation balance at the sea surface by altering atmospheric water vapor transport patterns. Today, there is net vapor transport from the Atlantic to Pacific [Broecker, 1992]. Results from a coupled ocean-atmosphere general circulation model indicate this pattern may change during intervals of low Atlantic thermohaline overturn. Surface cooling

due to a diminished "conveyor" results in less net evaporation from the northern Atlantic [Manabe and Stouffer, 1988]. Under these conditions, Atlantic to Pacific water vapor transport over Central America by tropical easterlies and Asia by northern westerlies should decrease, favoring greater Pacific salinity, as modeled by Manabe and Stouffer [1988]. We call this mechanism the "salt see-saw" -- the tendency for salt to accumulate in the surface North Pacific, lessening water column stability, when NADW production is low.

A strengthened East Asian winter monsoon would increase evaporation rates in the western Pacific near southeast Asia. Input of these waters to the northwest Pacific via the Kuroshio Current would also enhance the likelihood of deep ventilation. Consistent with this idea, data from the Chinese loess plateau imply that the strength of the winter monsoon increased near the time of stadial events [Porter and Zhisheng, 1995]. Although box model results from Warren [1983] indicate that the salinity of the Kuroshio Current would need to increase by more than 1.5‰ relative to today for deep water formation to occur, this effect, in concert with reduced Atlantic to Pacific vapor transport, may have yielded the salinity necessary for deep thermohaline overturn in the North Pacific.

2.6.5 Ventilation from Below

In the South Pacific and South Atlantic, water at depths of 2-3 km spreads south toward Antarctica to contribute to the so-called "Common Water", a major component of the world's deep water system [Broecker *et*

al., 1985]. What causes this flow? One idea is that mid-depth waters are drawn southward to compensate northward Ekman transport around Antarctica. Since water near the surface cannot flow south in the circumpolar region, due to a lack of topographic barriers, deeper water must counterbalance the Ekman process. Presently, North Atlantic Deep Water appears to be the primary source for this flow [Toggweiler and Samuels, 1995].

The demand for southward deep water advection at 2-3 km depth would occur whether or not NADW formed (such as during stadial intervals). At these times, the burden of compensating flow may shift to the Pacific, enhancing overturn of abyssal waters. This would decrease the residence time of NPDW, and thus increase its $\delta^{13}C$. In this scenario, reduced buoyancy forcing in the Atlantic, perhaps as a result of iceberg flux and melting, is automatically compensated by enhanced overturn in the deep Pacific. We call this mechanism the "Antarctic flywheel" -- the tendency for circumpolar winds to draw deep water from the Atlantic or the Pacific as necessary.

Unlike the "salt see-saw", the "flywheel" mechanism does not require deep water formation in the North Pacific, just enhanced turnover of deep and bottom waters. These two mechanisms are not mutually exclusive. Both depend on reduced NADW formation, and therefore could occur simultaneously. Isolating one of the two mechanisms will require comparison of W8709A-13PC $\delta^{13}C$ to high resolution records from intermediate and deep sites in the Pacific. Existing records from intermediate depths are consistent with the "salt see-saw mechanism", but

the current scarcity of high-resolution records from the deep Pacific precludes evaluation of the "Antarctic flywheel" idea.

2.6.6 Comparison to Shallower Pacific Records

During the last deglaciation, millennial-scale fluctuations in oxygenation occurred both at 700 m depth in the Gulf of California [Keigwin and Jones, 1990] and at 450 m depth in the Santa Barbara Basin [Kennett and Ingram, 1995]. Careful comparison of W8709A-13PC $\delta^{13}C$ and the Santa Barbara record during the Younger Dryas (YD) shows that deep NE Pacific ventilation lagged that of the intermediate-depth NE Pacific by at least 500 years, although the ventilation events overlap near the YD termination (Figure 2.5). This pattern is consistent with a joint "salt see-saw" and "Antarctic flywheel" scenario, in which changes in NADW production first affect the intermediate-depth N.E. Pacific via the atmosphere and then the deep N.E. Pacific via fluctuations in global thermohaline circulation.

Benthic foraminiferal Cd/Ca results from the California margin (core F8-90-G21) imply that ventilation decreased at 1600 m depth near the time of the Younger Dryas [van Geen *et al.*, 1996]. Unfortunately, dating uncertainties prevent a useful comparison of F8-90-G21 and W8709A-13PC. Core F8-90-G21 lacks chronological control from 11 to 16 ka [van Geen *et al.*, 1996] and the ^{14}C plateau at this time makes it difficult to compare time series unless the stratigraphic position of the plateau is constrained.

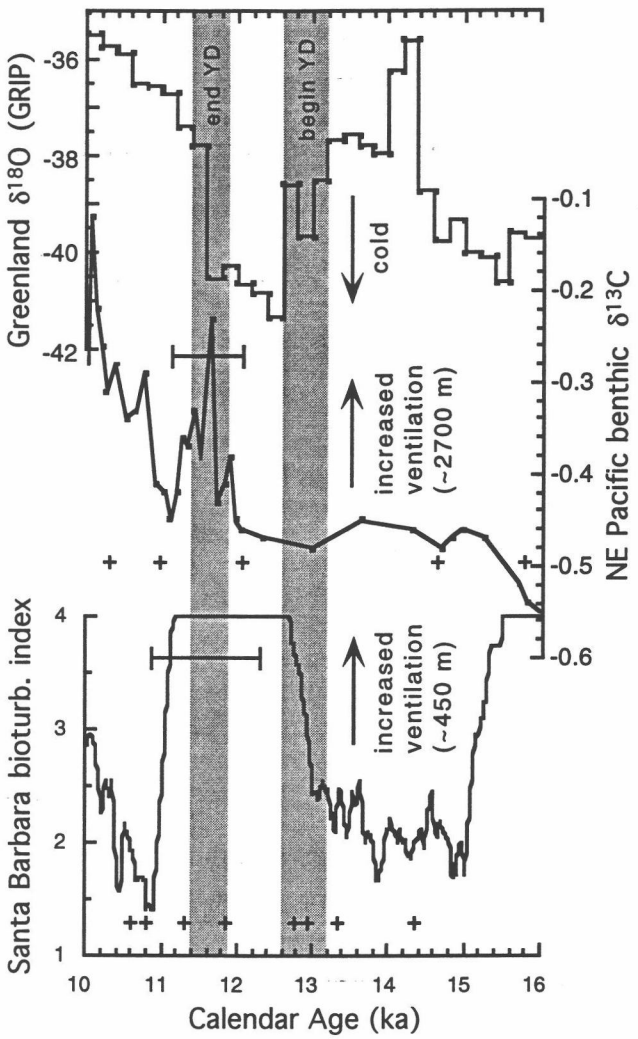

Figure 2.5 Comparison of W8709A-13PC $\delta^{13}C$, Santa Barbara Basin (ODP 893) bioturbation index [Behl and Kennett, 1996], and Greenland (GRIP) $\delta^{18}O$ [Dansgaard *et al.*, 1993] during the last deglaciation. In the GRIP record, the Younger Dryas (YD) begins at 12,700±100 yr BP and ends at 11,550±70 yr BP [Johnsen *et al.*, 1992], consistent with the YD age range in the GISP II ice core (12,940±250 to 11,640±250 yr BP; Alley *et al.* [1993]). ^{14}C control points (+) for W8709A-13PC and ODP 893 are indicated next to each time series. The $\delta^{13}C$ record reveals an interval of enhanced deep NE Pacific ventilation centered at 11.6 ka, near the end of the YD. This age range for this $\delta^{13}C$ peak (11.1-12.1 ka) indicates that deep NE Pacific ventilation lagged the YD initiation, and enhanced ventilation in the Santa Barbara Basin, by at least 500 years. Age uncertainty for the termination of the YD ventilation event in the Santa Barbara Basin (11.0-12.3 ka; Kennett and Ingram [1995]) precludes a detailed comparison to deep Pacific $\delta^{13}C$ in this interval, but it is likely that the ventilation events overlap.

From 15 to 60 ka, non-laminated intervals representing periods of high oxygen content in the Santa Barbara Basin seem to correlate with cold events in Greenland [Behl and Kennett, 1996]. Since we show that ventilation of the deep N.E. Pacific generally increased during stadial conditions, ventilation of the intermediate and deep Pacific may have been in phase during this time. Determining if the apparent ventilation lag during the Younger Dryas holds for earlier climatic events will require better age control in both W8709A-13PC and ODP 893 from 15-60 ka. Independent of chronology, however, our finding that millennial-scale $\delta^{13}C$ maxima generally occur during heavy $\delta^{18}O$ intervals (ice advance and deep-sea cooling) in W8709A-13PC implies the deep N.E. Pacific was better ventilated during stadial than interstadial conditions.

2.7 CONCLUSIONS

Stable isotopic variations recorded by *C. wuellerstorfi* in a core from the deep Northeast Pacific outline repeated millennial-scale deep water oscillations during the last glacial period. $\delta^{18}O$ highs appear to correlate to N. Atlantic stadial events, and are probably partially controlled by ice volume, implying $\delta^{18}O$ has potential as a high-resolution stratigraphic index. Enrichment of ^{13}C during $\delta^{18}O$ maxima suggests that intervals of strong ventilation in the deep Pacific occurred during ice advances, opposite the pattern in the deep N. Atlantic. Thus, during the last glacial period, there appears to be an alternating relationship between deep ventilation in the Pacific and the Atlantic on millennial time scales.

This relationship could be a function of two separate mechanisms, both of which are internal to earth's climate system. The first mechanism involves salt build-up and cooling in the North Pacific, decreased water column stability, and ventilation of the deep Pacific from above when the N. Atlantic cools. We call this the "salt see-saw." Alternatively, ventilation may have occurred from below, due to increased Pacific outflow compensating wind-driven northward advection in the Southern Ocean. We call this mechanism the "Antarctic flywheel". While data from intermediate depths in the Pacific (e.g., Santa Barbara Basin) are consistent with the "salt see-saw" scenario, the apparent lag (> 500 yr) of deep water ventilation behind intermediate water oxygenation during the Younger Dryas event suggests that the two mechanisms acted together.

2.8 ACKNOWLEDGEMENTS

We thank Candace Cloud, June Wilson and Ann Morey for help with sample preparation and Bill Rugh for operating the stable isotope mass spectrometer. We thank Michaele Kashgarian at Lawrence Livermore National Laboratory for the radiocarbon dates and Rick Behl, Jess Adkins, and Lex van Geen for reviewing the manuscript. This work was funded by NSF grant ATM 9632029 (to A.C.M.). Core material curation at Oregon State University was funded by NSF.

3.

Abrupt Deglacial Cooling Event in the N.E. Pacific Lags the Younger Dryas -- Are they Related?

David C. Lund and Alan C. Mix

College of Oceanic and Atmospheric Sciences
Oregon State University, Corvallis, Oregon

3.1 ABSTRACT

Planktonic foraminiferal faunal counts in the N.E. Pacific (~42°N, 126°W) reveal millennial-scale sea surface temperature (SST) change during the last deglaciation (10-18 cal ka). Modern analog SST estimates indicate a ~3°C cooling near the time of the North Atlantic Younger Dryas (YD) event. High-resolution ^{14}C dates that define the stratigraphic position of the deglacial radiocarbon "plateau" imply that N.E. Pacific cooling lagged the YD initiation by ~1 kyr. Biogenic opal, barium, and organic carbon data from the N.E. Pacific indicate reduced export productivity during the cooling event, making it unlikely that low SSTs were a response to enhanced coastal upwelling. We infer that the N.E. Pacific cool episode was associated with large-scale advection in the California Current. The apparent 1 kyr lag time of the Pacific event behind the N. Atlantic YD is not consistent with models that transmit the climate signal via the atmosphere. Another process must have been involved, such as slow response of regional ice cover that modified atmospheric circulation over the N.E. Pacific, or, more likely, northward surface heat transport linked to deep water formation in the North Pacific.

3.2 INTRODUCTION

Ice core and ocean sediment archives indicate the last deglaciation in the North Atlantic region was interrupted by a major cooling event, known as the Younger Dryas [Dansgaard *et al.*, 1993; Lehman and Keigwin, 1992; Bond and Lotti, 1995]. Climate records from the Northeast Pacific contain

climate oscillations similar to the YD, suggesting it was at least a hemispheric event [Keigwin and Jones, 1990; Kennett and Ingram, 1995; van Geen *et al.*, 1996]. The Younger Dryas may be triggered by ice sheet melt-water input to the N. Atlantic [Edwards *et al.*, 1993] and reduced North Atlantic Deep Water formation [Lehman and Keigwin, 1992]. Coupled ocean-atmosphere model results imply that YD climate change could have been communicated to the N.E. Pacific via atmospheric cooling in the mid- to high-latitudes of the Northern Hemisphere [Mikolajewicz *et al.*, 1997].

Here we present new evidence for an abrupt (~3°C) surface water cooling event in the N.E. Pacific during the last deglaciation. Pacific cooling is analogous to the Younger Dryas event in the circum-N. Atlantic region, but appears to lag that in the Atlantic by ~1 kyr. We offer two possible climate mechanisms to explain this phenomenon, one which entails changes in atmospheric circulation related to the height of the Laurentide Ice Sheet, and one which involves deep water formation and poleward heat transport in the N. Pacific.

3.3 MODERN OCEANOGRAPHIC SETTING

The sediment core used for this study, W8709A-13PC (2712 m depth; 42.1°N, 125.8°W) is located 120 km off the coast of southern Oregon, near the eastern edge of the California Current (Figure 3.1). The California Current is a diffuse, 600-700 km wide, eastern boundary current that carries about 10 Sv of cold, low salinity subarctic water southward along the coast of North America [Sverdrup *et al.*, 1942].

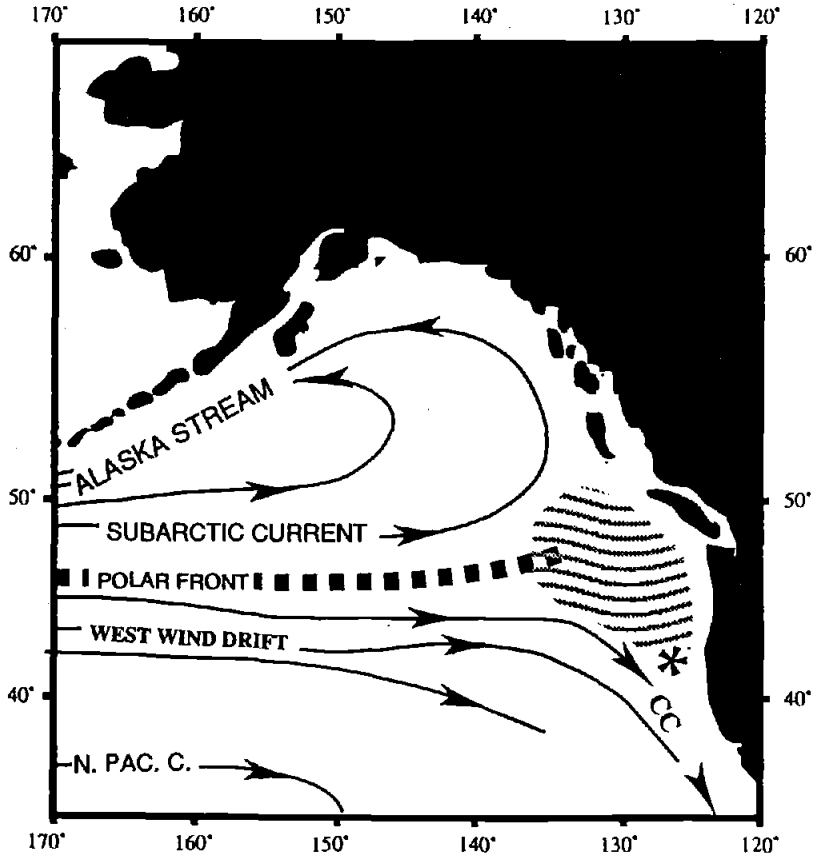

Figure 3.1 Location of W8709A-13PC (42°N, 126°W) relative to major oceanographic currents in the Northeast Pacific Ocean. The core is located on the eastern edge of the California Current (CC), approximately 120 km from the coast of North America. The striped zone represents the region of West Wind Drift divergence. Modified from Gardner *et al.* [1997].

Coastal upwelling at 42°N is strongest during the spring and summer months, due to strong northwesterly winds which form on the eastern edge of the North Pacific High (NPH), and weakest during the winter months, due to displacement of the NPH by the Aleutian Low [Huyer, 1983]. Upwelling brings colder, more saline, nutrient-rich water to the surface, fueling primary production and producing chlorophyll maxima parallel to the coast [Atlas *et al.*, 1978; Huyer, 1983]. Active upwelling is restricted to a 10-25 km wide zone, though at 42°N a major cold water filament and its associated mesoscale eddy carry upwelled water to greater than 200 km offshore [Ikeda and Emery, 1984; Strub *et al.*, 1991]. Seasonal variations in open ocean upwelling due to positive wind stress curl reinforce the coastal upwelling pattern [Huyer, 1983], but the two processes may have been decoupled on glacial-interglacial time scales [Ortiz *et al.*, 1997].

3.4 METHODS

3.4.1 Chronostratigraphy

The age model used for W8709A-13PC is the "average" age model discussed in Chapter 2. Since the focus of this chapter is from 8-18 ka, the chronology is based entirely on calendar-corrected ^{14}C dates.

3.4.2 Sea-surface Temperature

Samples were picked for planktonic foraminifera at 6 cm intervals from 99 to 136 cm and 227 to 298 cm and 3 cm intervals from 136 to 227 cm

in W8709A-13PC. Foraminifera >150 μm in size were identified to species level using standard CLIMAP taxonomic categories [Saito *et al.*, 1981; Parker, 1962]. We do not recognize the *P-D* intergrade category of Kipp [1976] in this study. Qualitative estimates of sea-surface temperature (SST) were made by calculating the percentage of left-coiling *N. pachyderma* relative to the total number of *N. pachyderma* [left(L) + right-coiling(R)], called the *N. pachyderma* coiling percentage, in each sample. Where summer SSTs are less than 5°C, the *N. pachyderma* core-top population is generally comprised of 95% left-coiling variety. Above 10°C, *%N. pachyderma (L)* approaches zero [Be *et al.*, 1971].

We used the modern analog technique (MAT) of Hutson [1980] to quantitatively estimate SST. The MAT compares down-core planktonic foraminiferal assemblages with a core top data base to find the least dissimilar modern assemblages. The SST for the ancient assemblage is calculated by averaging the modern SSTs for the five least dissimilar core tops. Underlying this method are two critical assumptions, 1) that similar environmental conditions produce similar assemblages, and 2) that temperature, or variables correlated to temperature, exert the primary control on faunal composition. We calculated modern analog SSTs using the squared chord distance technique, a dissimilarity threshold of 0.15, and the global core top database (n=1121) used by Ortiz and Mix [1997]. Of the 45 samples in W8709A-13PC picked for planktonic foraminifera, all had average dissimilarity coefficients <0.15 and three were >0.12.

The MAT has the advantage of providing a quantitative estimate of temperature, but the disadvantage of possible sensitivity to preservation in

the region [Ortiz *et al.*, 1997]. The *N. pachyderma* coiling percentage is relatively insensitive to variable preservation, but does not scale linearly to temperature. Thus, we illustrate changes in both indices.

3.5 RESULTS

All planktonic foraminiferal species percentages vary significantly from 99-280 cm in W8709A-13PC. *N. pachyderma (L)*, the predominant species, ranges from 50% during marine oxygen isotope stage 2 (MIS 2) to <20% in MIS 1 (Figure 3.2b). The maximum percentage of *N. pachyderma (L)* (greatest cooling) occurs at 150 cm. *G. bulloides* shows a steady decrease from ~40% in stage 2 to <5% in stage 1 (Figure 3.2c), while *N. pachyderma (R)* has an opposite pattern, increasing from ~0% at the Last Glacial Maximum (250-300 cm depth) to nearly 50% in the Holocene (Figure 3.2d). There is a large decrease in %*N. pachyderma (R)* centered at 150 cm.

The coiling percentage of *N. pachyderma* (Figure 3.3a) implies an SST increase near the MIS 1-2 boundary, then an abrupt SST decrease from 175 to 150 cm. This ~30% cooling transition is equal to the full glacial-interglacial change in coiling ratio at this site [Ortiz *et al.*, 1997]. Modern analog SST estimates (Figure 3.3b) indicate surface water temperatures of ~10°C during the LGM, in agreement with previous foraminiferal- [Ortiz *et al.*, 1997] and radiolaria-based methods [Sabin and Pisias, 1996]. SSTs warmed to ~11°C near the MIS 1-2 boundary, cooled to ~8°C beginning at 180 cm, and then rebounded to ~11°C at 125 cm. The coiling percentage of *N. pachyderma* and

modern analog SST estimates reveal a major cooling event that interrupts the glacial-interglacial transition in the N.E. Pacific.

3.6 DISCUSSION

3.6.1 Advection vs. Upwelling

Sea-surface temperature at 42°N, 126°W is a function of large-scale California Current advection and local wind-driven changes in upwelling. If the deglacial cooling event was a function of enhanced coastal upwelling, then it should be associated with high values in proxies of export productivity. Biogenic opal and organic carbon values decrease in the interval of low SST (~140-175 cm), opposite the pattern expected if coastal upwelling drove changes in SST (Figure 3.3). Low levels of biogenic barium from in this interval [J. Gardner, unpublished results] are consistent with the opal and organic carbon data. Since cooling appears to be associated with lower export productivity in W8709A-13PC, we infer that the low SSTs from ~140-175 cm were a function of large scale advection in the California Current rather than local coastal upwelling effects.

This pattern of low SST and low export productivity is analogous to Last Glacial Maximum (LGM) conditions in a transect of cores at 42°N, across the California Current. Diatom spores, biogenic silica and barium, and marine organic carbon at 126°W (W8709A-13PC), 128°W, and 132°W indicate that export productivity was roughly half modern levels during the LGM [Lyle *et al.*, 1992; Sancetta *et al.*, 1992], when SSTs were approximately

Figure 3.2 Benthic $\delta^{18}O$ and planktonic species abundance vs. depth in W8709A-13PC. (A) $\delta^{18}O$ samples above 100 cm depth are *Uvigerina spp.* (*U. senticosa* and *U. peregrina*). *C. wuellerstorfi* $\delta^{18}O$ values were adjusted by +0.64 to match the *Uvigerina* scale. Marine oxygen isotope stages 1 and 2 are indicated on the upper x-axis. (B-G) Species percent abundance, including *N. pachyderma (L), G. bulloides, N. pachyderma (R), G. quinqueloba, N. dutertrei,* and *G. glutinata.* Percentage values are listed in Appendix B.

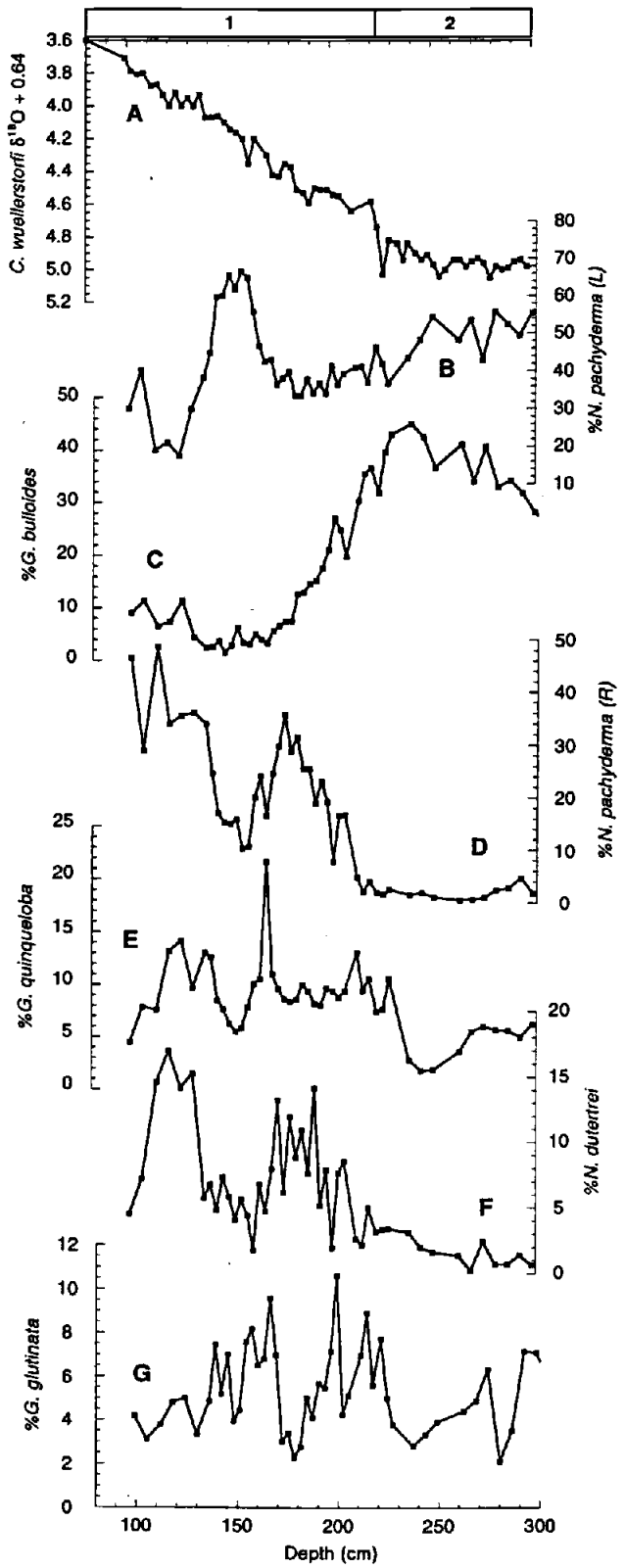
1
2
C. wuellerstorfi δ18O + 0.64
A
%N. pachyderma (L)
B
%G. bulloides
C
%N. pachyderma (R)
D
%G. quinqueloba
E
%N. dutertrei
F
%G. glutinata
G
Depth (cm)

Figure 3.2

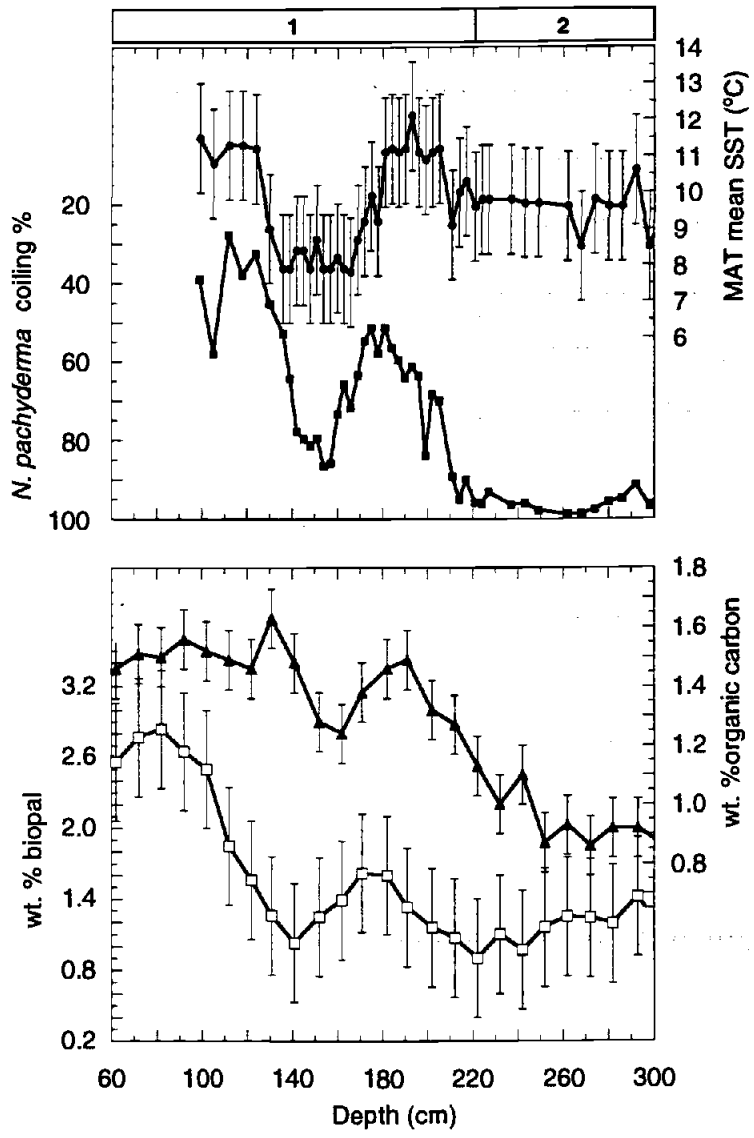

Figure 3.3 The percentage of *N. pachyderma (L)* relative to the total number of *N. pachyderma (L+R)* (solid squares), modern analog mean sea-surface temperature (solid circles), weight percent biogenic opal (open squares), and weight percent organic carbon (solid triangles) vs. depth in W8709A-13PC. Marine oxygen isotope stages 1 and 2 are indicated on the uppermost x-axis. Both temperature proxies indicate significant cooling centered at 150 cm, and both opal and organic carbon imply reduced export productivity during the cold event. RMS error for the modern analog temperature estimates is ±1.5°C [Ortiz *et al.*, 1997]. Error for the opal and organic carbon measurements is ±0.5% and ±0.1%, respectively [Gardner *et al.*, 1997].

4°C cooler than at present [Ortiz *et al.*, 1997; Prahl *et al.*, 1995]. Global paleoclimate simulations imply the LGM North Pacific High was significantly weaker than today, while the Aleutian low was stronger [Kutzbach, 1987; COHMAP, 1988], favoring onshore winds, and low coastal upwelling, consistent with LGM export productivity proxies. Biogenic opal and barium, and to a lesser extent organic carbon, imply atmospheric circulation patterns from 140-175 cm were similar those at the LGM.

3.6.2 Timing of Events

The relative timing of deglacial climate oscillations in the Atlantic and Pacific is critical for understanding the mechanisms responsible for global registration of the Younger Dryas cold interval. Synchronous events in the two basins would imply connection via the atmosphere, which is capable of rapid response to climate change. A time lag would implicate continental ice sheets or the deep sea, which are inherently slower teleconnection pathways. In Figure 3.4, the coiling percentage of *N. pachyderma*, modern analog SST estimates, and Greenland (GRIP) ice core $\delta^{18}O$ [Dansgaard *et al.*, 1993] are plotted vs. calendar age. In the GRIP record, the YD begins at 12,700±100 yr BP and ends at 11,550±70 yr BP [Johnsen *et al.*, 1992], consistent with the YD age range in the GISP II ice core (12,940±250 to 11,640±250 yr BP; Alley *et al.* [1993]).

The coiling percentage of *N. pachyderma* reveals an interval of cooling beginning at 11.7 ka, approximately 1.1 kyr after the YD initiation in Greenland. The age range for the beginning of the SST cooling (11.3-12.1),

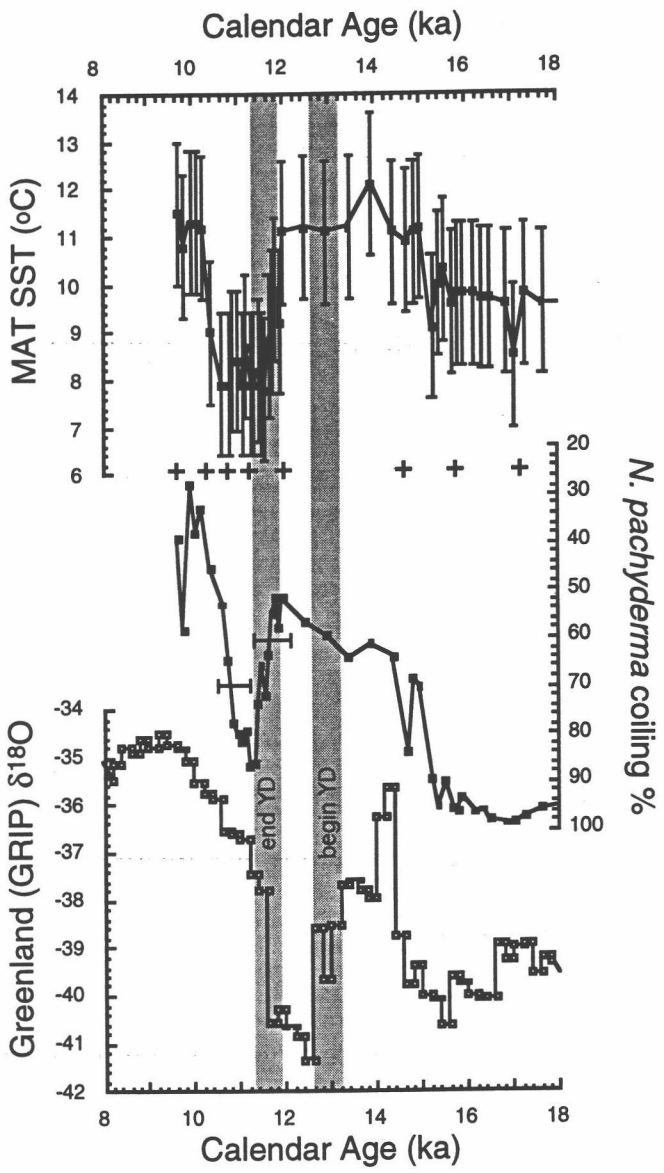

Figure 3.4 N.E. Pacific modern analog SST estimates, *N. pachyderma* coiling percentage, and Greenland (GRIP) $\delta^{18}O$ [Dansgaard et al., 1993] vs. calendar age. The shaded areas represent the age range for the beginning and end of the Younger Dryas (see text). ^{14}C control points (+) for W8709A-13PC are located next to the SST time series. The *N. pachyderma* coiling percentage reveals an interval of SST cooling beginning at 11.7 ka (11.3-12.1), lagging the YD initiation by >500 years. The end of the N.E. Pacific SST event occurred at 10.8 ka (10.5-11.3 ka), >100 years after the YD termination. The age ranges for the beginning and end of the N.E. Pacific cold interval are represented by horizontal bars.

constrained by the age model options in Figure 2.1b, implies that N.E. Pacific cold event lagged the YD initiation (including ice core dating uncertainty) by at least 500 years. The end of the N.E. Pacific event occurred at 10.8 ka, about 800 years after the YD termination, although uncertainty for the end of the N.E. Pacific cooling (10.5-11.3 ka) and for the end of the YD (11.4-11.9 ka) indicates temperature shifts in the two regions may have been synchronous. The relative timing of events in Greenland and the N.E. Pacific does not change significantly if modern analog SST estimates, rather than the coiling percentage of *N. pachyderma*, are compared to the YD ice core chronology.

As a second check on the timing of Pacific temperature change, we plotted the *N. pachyderma* coiling percentage against the age model for W8709A-13PC (Figure 3.5). Reservoir-corrected radiocarbon dates indicate the beginning of the deglacial ^{14}C "plateau" [Stuiver and Braziunas, 1993] is at or below 180 cm depth. Since SSTs decrease starting at 175 cm and the calendar age for the beginning of the plateau is 11.9-12.3 ka [Bard *et al.*, 1993; Edwards *et al.*, 1993], we know that cooling in the N.E. Pacific began after 12.3 ka. Although it is possible that reservoir ages changed in the N.E. Pacific, this would not significantly alter the stratigraphic position of the ^{14}C plateau. Thus, N.E. Pacific cooling must have lagged N. Atlantic cooling by a significant amount, at least 500 years and perhaps more than 1 kyr.

The major cold-warm transition at ~140 cm in W8709A-13PC occurs within the possible range of depths for end of the ^{14}C plateau (134-154 cm). Although it appears that the plateau could end below the age-control point at 139 cm, making the calendar age for the cold-warm transition 11.5 ka (Table 1), this date falls within the calendar age range for the ^{14}C plateau

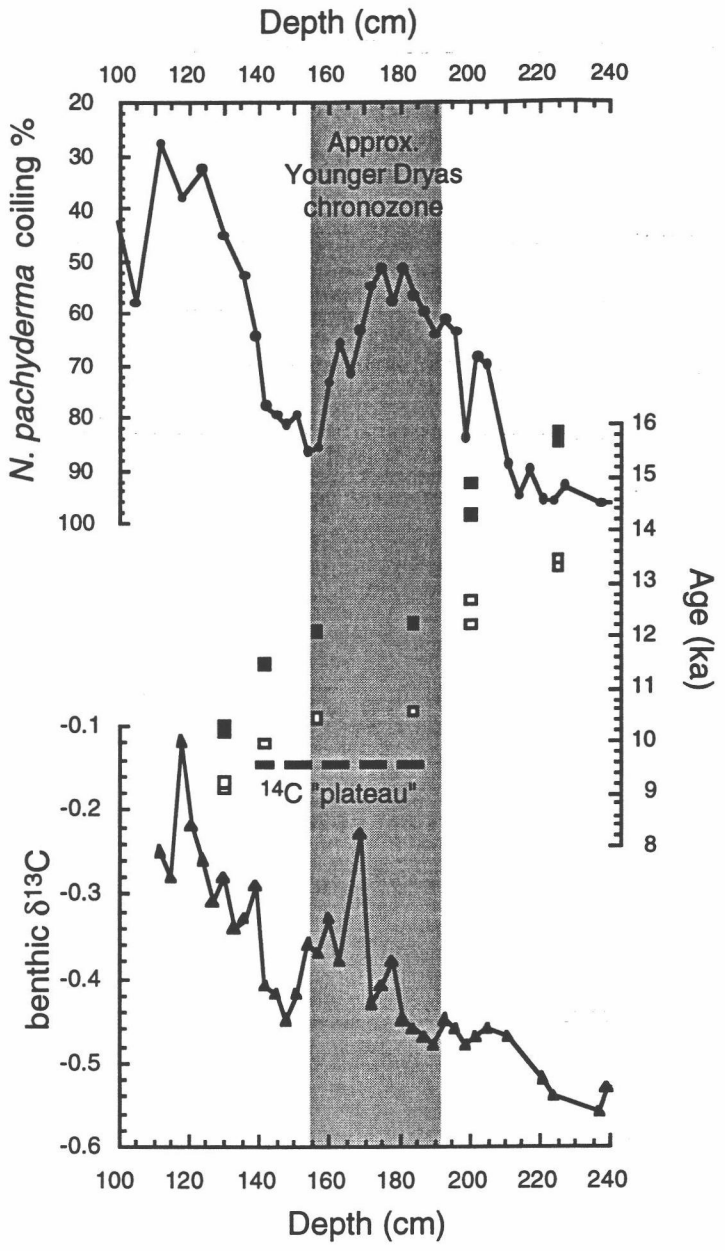

Figure 3.5 *N. pachyderma* coiling percentage (solid circles), reservoir-corrected ^{14}C ages (open squares) and calendar ages (solid squares), and *Cibicidoides wuellerstorfi* $\delta^{13}C$ (solid triangles) vs. depth in W8709A-13PC. The beginning of the deglacial ^{14}C "plateau", at 11.9-12.3 ka [Stuiver and Braziunas, 1993; Edwards *et al.*, 1993], occurs at or below 180 cm, indicating SST cooling in the N.E. Pacific occurred after 12.3 ka. The shaded area represents the approximate depth equivalent of the Younger Dryas chronozone (~11.6-12.8 ka). The $\delta^{13}C$ peak from ~150-180 cm corresponds to the deglacial ^{14}C "plateau", and in general, high $\delta^{13}C$ occurs during intervals of high SST.

[Stuiver and Braziunas, 1993; Edwards *et al.*, 1993]. Therefore, the end of the cold interval in the N.E. Pacific occurred near the end of the ^{14}C plateau, and likely post-dates the YD termination.

3.6.3 Atlantic-Pacific Climate Teleconnections

3.6.3.1 Atmospheric

Altering the strength of southward-flowing North Atlantic Deep Water (NADW), and hence the warm northward-flowing, surface waters which compensate NADW, dramatically affects sea-surface temperature in the Northern Hemisphere. Coupled ocean-atmosphere simulations using modern boundary conditions predict that shut-down of Atlantic thermohaline circulation cools the northern North Atlantic by an average of 4°C [Manabe and Stouffer, 1988; Mikolajewicz *et al.*, 1997]. Simulated temperature change in the N. Pacific (1-2°C) lags that in the N. Atlantic by ~100 years. Along the west coast of N. America, modeled surface water cooling is less intense (<1°C), as a result of anomalously strong onshore winds and downwelling in this region [Mikolajewicz *et al.*, 1997].

If the Younger Dryas was related to decreased NADW production, as suggested by paleoceanographic proxies [Boyle and Keigwin, 1987; Lehman and Keigwin, 1992], and model results accurately depict Northern Hemisphere registration of the event, we should expect a subtle (<1°C) cooling in the N.E. Pacific near 12.8 ka (the YD initiation). Instead, we observe constant or increasing SST at 12.8 ka, followed by a decrease of ~3°C

beginning at 11.7 ka. The timing of the N.E. Pacific cooling event implies that it is a delayed response to YD-related climate change.

The climate simulations of Manabe and Stouffer [1988] and Mikolajewicz *et al.* [1997] use the modern, rather than deglacial extent, of continental ice sheets and therefore may not accurately depict conditions in the N.E. Pacific during the last deglaciation. Models which include the effect of N. American continental ice show dramatically different weather patterns over North America relative to modern conditions. For example, COHMAP [1988] results imply the westerly jet stream was split into two major branches, with one limb passing over the Laurentide Ice Sheet, and one over the southwestern United States. Abrupt decreases in ice sheet elevation (associated with ice-rafting events) may have allowed Arctic air masses to penetrate further south, cooling much of N. America [Hostetler *et al.*, in press].

Although simulated cooling and anomalous downwelling in the N.E. Pacific during the Younger Dryas [Mikolajewicz *et al.*, 1997] is consistent with changes observed in W8709A-13PC from 10.8-11.7 ka, the timing and magnitude of modeled SST change does not match the paleoceanographic record. The apparent ~1 kyr lag time between the N. Atlantic and N.E. Pacific implies that atmospheric cooling due to the direct effects of reduced NADW formation exerted little influence on N.E. Pacific SST at the Younger Dryas initiation. The smaller age offset for the YD termination and SST warming implies the atmosphere may have played a more prominent role at this time.

3.6.3.2 Cryospheric

The cryosphere generally responds to climate change more slowly than the atmosphere, and therefore may play a part in the apparent delay between Greenland and N.E. Pacific temperature records. Many of the so-called "Heinrich" ice rafting events from 15-60 ka lag millennial-scale warm-cold transitions in the N. Atlantic by >1 kyr [Bond *et al.*, 1993]. If Heinrich-scale reductions in Laurentide Ice Sheet elevation cause surface cooling in the N.E. Pacific, as suggested by simulated post-Heinrich event-2 atmospheric circulation patterns [Hostetler *et al.*, in press], then analogous changes in ice sheet size during the Younger Dryas, as a result of Heinrich event-0 (H-0), may have indirectly influenced N.E. Pacific sea-surface temperatures.

The >50 m increase in sea level from 25 ka (H-2) to 13 ka [Fairbanks, 1990; Bard *et al.*, 1996] indicates continental ice volume during the Younger Dryas was roughly half that of the Last Glacial Maximum (LGM). Lithic grain concentrations (a tracer of ice berg flux) in the N. Atlantic are ~75% lower for H-0 than for H-events 1, 2, and 4, implying H-0 caused a smaller change in ice-sheet size than the earlier ice rafting episodes [Bond and Lotti, 1995]. Heinrich event-2 atmospheric effects simulated by Hostetler *et al.* [in press] using LGM boundary conditions may not occur when the continental ice volume is relatively low, such as during the Younger Dryas.

Lithic grain and detrital carbonate concentrations (also a tracer of iceberg flux) indicate H-0 began synchronously with Younger Dryas SST cooling in the N. Atlantic [Bond and Lotti, 1995; Andrews *et al.*, 1995], in

contrast to the pattern for earlier Heinrich events. Unless changes in atmospheric circulation occurred towards the end of H-0, ~750 years after the YD initiation [Bond and Lotti, 1995], ice-sheet related temperature effects in the N.E. Pacific would occur at ~12.8 ka rather than 11.7 ka. A massive ice melting event at ~11.0 ka [Fairbanks, 1990; Edwards *et al.*, 1993], apparently independent of H-0, may have reduced ice sheet elevation significantly, but the event postdates cooling in the N.E. Pacific. Thus, the magnitude and timing of deglacial ice sheet decay does not seem consistent with an ice-elevation related change in N.E. Pacific surface temperatures.

3.6.3.3 Oceanic

Similar to the cryosphere, the deep ocean responds to climate change more slowly than the atmosphere, raising the possibility that the N. Atlantic Younger Dryas event was communicated to the N.E. Pacific via global thermohaline circulation. Benthic foraminiferal $\delta^{13}C$ data in W8709A-13PC indicate enhanced deep N.E. Pacific ventilation near the SST transition at ~150-180 cm (Figure 3.5). This $\delta^{13}C$ peak occurs during the deglacial radiocarbon "plateau". The ~150 per mil decrease in atmospheric $\Delta^{14}C$ from 12.3-11.0 cal ka, which accounts for the ^{14}C plateau, is thought to be due to enhanced turnover of the deep ocean [Edwards *et al.*, 1993]. The coincidence of the plateau with high $\delta^{13}C$ supports the idea that the $\delta^{13}C$ peak represents increased ventilation of the deep N. Pacific.

The strength of deep thermohaline overturn may affect atmospheric water vapor inventory and hence surface temperatures via greenhouse

warming [Broecker, 1994]. This mechanism, however, would likely influence the entire globe, and doesn't account for the apparent N. Atlantic-N.E. Pacific lag, unless the N. Atlantic responds primarily to direct regional effects of reduced NADW formation, and the N.E. Pacific to its indirect global effects. Alternatively, deep water formation in the N. Pacific during the Younger Dryas may have created a thermohaline cell analogous to the modern Atlantic, carrying warm surface waters to high latitudes in the Pacific, and delaying cooling of the N.E. Pacific until after the Younger Dryas event.

3.7 CONCLUSIONS

A high-resolution sea-surface temperature record from the N.E. Pacific implies that SSTs decreased ~3°C at 11.7 ka, nearly ~1 kyr after the Younger Dryas (YD) initiation in Greenland ice cores. Minimum Atlantic-Pacific lag time, constrained by the stratigraphic position of the deglacial ^{14}C plateau, is 500 years. Thus, cold events interrupting the deglaciation are not necessarily coeval with the YD chronozone.

Proxies of export productivity indicate the N.E. Pacific SST cooling was probably a function of large-scale advection in the California Current rather than local changes in coastal upwelling. The ~1 kyr lag time between the YD initiation and low SST at 42°N, 126°W is not consistent with coupled-ocean atmosphere models which simulate rapid atmospheric transmission of N. Atlantic temperatures to the N.E. Pacific. A slower teleconnection pathway must have been involved.

Although reduced N. American ice sheet elevation during the Younger Dryas, and related changes in atmospheric circulation, could have caused SST cooling in the N.E. Pacific, the magnitude and timing of H-0 seems inconsistent with this scenario. Instead, we speculate that deep water formation in the N. Pacific created a thermohaline cell similar to the modern N. Atlantic. The advection of warm, low latitude surface waters to the N.E. Pacific likely obscured cooling related to the downwind effects of low North Atlantic Deep Water production during the Younger Dryas.

3.8 ACKNOWLEDGEMENTS

We thank Ann Morey for help with species identification and modern analog SST estimates and Bill Rugh for ^{14}C sample preparation. This work was funded by NSF grant ATM 9632029 (to A.C.M.). Core material curation at Oregon State University was funded by NSF.

4.

Summary

4.1 Primary Results

Three goals were outlined at the beginning of this thesis: (1) to use benthic foraminiferal stable isotopes to determine if millennial-scale climate oscillations affected the deep N.E. Pacific, (2) to characterize sea-surface temperatures during the last deglaciation using planktonic foraminiferal assemblages, and (3) to compare N.E. Pacific data to paleoclimate archives from the N. Atlantic region to evaluate potential climate change mechanisms. The first goal was addressed in Chapter 2, the second in Chapter 3. The third goal was addressed at the end of each chapter. The purpose of this section is to summarize the primary results of this thesis.

Benthic foraminiferal $\delta^{18}O$ and $\delta^{13}C$ in core W8709A-13PC (42°N, 126°W; 2700 m depth) outline repeated millennial-scale flushing events of the deep N.E. Pacific during the last glacial period. Episodes of deep water nutrient depletion and/or increased air-sea gas exchange ($\delta^{13}C$ maxima) imply that enhanced ventilation generally occurred during intervals of ice growth and/or deep-sea cooling ($\delta^{18}O$ maxima). This is opposite the pattern observed in the N. Atlantic, where deep water production apparently decreased during stadial conditions. Radiocarbon and oxygen-isotope chronologies in W8709A-13PC support the apparent alternating relationship between deep ventilation in the Pacific and Atlantic on millennial time-scales.

We offer two mechanisms to explain the observed changes in benthic stable isotopes. The first, or "salt see-saw", involves deep water formation

in the N. Pacific, due to surface water cooling from downwind effects of low Atlantic thermohaline overturn, and enhanced surface salinity, as a result of reduced Atlantic-Pacific vapor transports. Alternatively, deep water change in the two basins may have been linked through the Southern Ocean. Due to bathymetric constraints around Antarctica, upwelling occurs from depths >1.5 km. Currently, the major source of upwelled waters is North Atlantic Deep Water (NADW). Intervals of low NADW production (i.e. stadial conditions) may have been compensated by increased Pacific mid-depth (2-3 km) outflow, ventilating the deep Pacific from below, rather than above. We call this mechanism the "Antarctic flywheel."

Comparison of W8709A-13PC benthic $\delta^{13}C$ to the Santa Barbara Basin bioturbation index implies deep ventilation lagged intermediate ventilation in the N.E. Pacific by >500 years. This lag time is consistent with a dual "salt see-saw" and "Antarctic flywheel" mechanism, where the consequences of low NADW production first affect intermediate depths in the N.E. Pacific via the atmosphere, and then the deep N.E. Pacific via thermohaline circulation.

Planktonic foraminiferal assemblages reveal a major cooling event in the N.E. Pacific that interrupts the last deglaciation. Modern analog sea-surface temperature (SST) estimates imply waters were ~3°C from 10.8-11.7 ka. Age uncertainty in this interval, constrained by the stratigraphic position of the deglacial radiocarbon "plateau" in W8709A-13PC, indicates N.E. Pacific cooling lagged the Younger Dryas initiation in Greenland ice cores by a minimum of 500 years. Thus, cold events interrupting the deglaciation are not necessarily coeval with the Younger Dryas chronozone.

The Atlantic-Pacific time lag is not consistent with an atmospheric teleconnection for the Younger Dryas (YD) event. Models of YD-like reductions in NADW production simulate synchronous SST change in the two basins. Apparently these models are hampered by their use of modern, rather than deglacial, boundary conditions. Reduced N. American ice sheet elevation during the Younger Dryas, and associated changes in atmospheric circulation, may have caused delayed SST response in the N.E. Pacific. The timing and magnitude of ice rafting/melting at this time, however, seems inconsistent with a cryosphere-related mechanism.

Lagged sea-surface temperature change in the N.E. Pacific during the Younger Dryas was most likely a function of thermohaline circulation. Enhanced ventilation in the N.E. Pacific ($\delta^{13}C$ maxima) during the deglaciation appears to occur during warm SST intervals. One possibility is that deep water formed in the N. Pacific at these times, similar to the modern N. Atlantic. As a result, warm, northward flowing surface waters from lower latitudes may have compensated deep southward flow.

4.2 Future Directions

Further millennial-scale paleoceanographic research is necessary to address issues raised in this thesis. First, this study focused on one sedimentary core which may be susceptible to local effects not present at other locations. Additional work should include similar high-sedimentation rate sites in the deep N.E. Pacific to verify the results presented here.

Determining the sequence of events at different geographic locations requires high-resolution radiocarbon dates, particularly during the last deglaciation, when atmospheric ^{14}C activity varied greatly. By defining the stratigraphic position of the radiocarbon "plateau" in W8709A-13PC, we demonstrated that a major cooling event in the N.E. Pacific lagged the Younger Dryas in the N. Atlantic, implying the atmosphere was not the primary teleconnection pathway at this time. Future paleoclimate studies must be chronologically well-defined to constrain mechanisms of millennial-scale climate change.

New modeling efforts are required to simulate Late Pleistocene climatic conditions in the N. Pacific. Ideally, models should couple the atmosphere, ocean, and ice sheets and utilize boundary conditions matching those of the time interval in question. In particular, a coupled ocean-atmosphere model of the Younger Dryas event, which includes the effects of variable ice sheet topography and deglacial boundary conditions, would help determine if ice elevation changes can realistically affect N.E. Pacific surface temperatures and whether deep water formation could have occurred in the N. Pacific during the last deglaciation.

BIBLIOGRAPHY

Alley, R. B., D. A. Meese, C. A. Shuman, A. J. Gow, K. C. Taylor, P. M. Grootes, J. W. C. White, M. Ram, E. D. Waddington, P. A. Mayewski, and G. A. Zielinski, Abrupt increase in Greenland snow accumulation at the end of the Younger Dryas event, *Nature, 362*, 527-529, 1993.

Andrews, J. T., A. E. Jennings, M. Kerwin, M. Kirby, W. Manley, G. H. Miller, G. Bond, and B. MacLean, A Heinrich-like event, H-0 (DC-0): Source(s) for detrital carbonate in the North Atlantic during the Younger Dryas chronozone, *Paleoceanography, 10*, 943-952, 1995.

Atlas, E. L., Gordon, L. I. and R. D. Tomlinson, Chemical characteristics of Pacific northwestern coastal waters--nutrients, salinities, seasonal fluctuations, in *The Marine Plant Biomass of the Pacific Northwest Coast*, edited by R. Krauss, 57-79, Oregon State University, Corvallis, 1978.

Bard, E., M. Arnold, and B. Hamelin, Present status of the radiocarbon calibration for the late Pleistocene (abstract), Fourth International Conference on Paleoceanography, *GEOMAR Report, 15*, 52-53, 1992.

Bard, E., M. Arnold, R. G. Fairbanks, and B. Hamelin, ^{230}Th-^{234}Th and ^{14}C ages obtained by mass spectrometry on corals, *Radiocarbon, 36*, 191-199, 1993.

Bard, E., B. Hamelin, M. Arnold, L. Montaggioni, G. Cabioch, G. Faure, and F. Rougerie, Deglacial sea-level record from Tahiti corals and the timing of global meltwater discharge, *Nature, 382*, 241-244, 1996.

Bard, E., F. Rostek, and C. Sonzogni, Interhemispehric synchrony of the last deglaciation inferred from alkenone palaeothermometry, *Nature, 385*, 707-710, 1997.

Baumgartner, A., and E. Reichel, *The World Water Balance: Mean Annual Global, Continental and Maritime Precipitation, Evaporation and Run-off*, 179 pp. Elsevier, Amsterdam, 1975.

Be, A. W., and D. S. Tolderlund, Distribution and ecology of living planktonic foraminifera in surface waters of the Atlantic and Indian oceans, in *Micropaleontology of Oceans*, edited by B. M. Funnell and W. R. Riedel, 105-149, Cambridge University Press, New York, 1971.

BIBLIOGRAPHY (continued)

Behl, R. J., and J. P. Kennett, Brief interstadial events in the Santa Barbara basin, NE Pacific, during the past 60 kyr, *Nature, 379*, 243-246, 1996.

Bond, G., W. Broecker, S. Johnsen, J. McManus, L. Labeyrie, J. Jouzel, and G. Bonami, Correlations between climate records from North Atlantic sediment and Greenland Ice, *Nature, 365*, 143-147, 1993.

Bond, G., and R. Lotti, Iceberg discharges into the North Atlantic on millennial time scales during the last glaciation, *Science, 267*, 1005-1010, 1995.

Boyle, E. A., and L. G. Keigwin, North Atlantic thermohaline circulation during the past 20,000 years linked to high-latitude surface temperature, *Nature, 330*, 35-40, 1987.

Broecker, W. S., D. W. Spencer, and H. Craig (Eds.), *GEOSECS Pacific Expedition, Volume 3, Hydrographic Data 1973-1974*, National Science Foundation, Washington, D. C., 1982.

Broecker, W. S., T. Takahashi, and T. Takahashi, Sources of flow patterns of deep-ocean waters as deduced from potential temperature, salinity, and initial phosphate concentration, *Journal of Geophysical Research, 90*, 6925-6939, 1985.

Broecker, W. S., and E. Maier-Reimer, The influence of air and sea exchange on the carbon isotope distribution in the sea, *Global Biogeochemical Cycles, 6*, 315-320, 1992.

Broecker, W. S., The Great Ocean Conveyor, in *AIP Conference Proceedings 247: Global warming: physics and facts*, edited by B. G. Levi, et al., pp. 129-161, American Institute of Physics, 1992.

Broecker, W. S., Massive iceberg discharges as triggers for global climate change, *Nature, 372*, 421-424, 1994.

Chappell, J., and N. J. Shackleton, Oxygen isotopes and sea level, *Nature, 324*, 137-140, 1986.

Chappell, J., Omura, A., Esat, T., McCulloch, M., Pandolfi, J., Ota, Y., and B. Pillans, Reconciliation of late Quaternary sea levels derived from coral terraces at Huon Peninsula with deep sea oxygen isotope records, *Earth and Planetary Science Letters, 141*, 227-236, 1996.

BIBLIOGRAPHY (continued)

COHMAP Members, Climatic changes of the last 18,000 years: Observations and model simulations, *Science, 241*, 1043-1052, 1988.

Corliss, B. H., Microhabitats of benthic foraminifera within deep-sea sediments, *Nature, 314*, 435-438, 1985.

Curry, W. G., J. C. Duplessy, L. D. Labeyrie, and N. J. Shackleton, Changes in the distribution of $\delta^{13}C$ of deep water ΣCO_2 between the last glaciation and the Holocene, *Paleoceanography, 3*, 317-341, 1988.

Curry, W. B., and D. W. Oppo, Synchronous, high-frequency oscillations in tropical sea surface temperatures and North Atlantic Deep Water production during the last glacial cycle, *Paleoceanography, 12*, 1-14, 1997.

Dansgaard, W., S. J. Johnsen, H. B. Clausen, D. Dahl-Jensen, N. S. Gunderstrup, C. U. Hammer, C. S. Hvidberg, J. P. Steffensen, A. E. Sveinbjornsdottir, J. Jouzel, and G. Bond, Evidence for general instability of climate from a 250-kyr ice-core record, *Nature, 364*, 218-220, 1993.

Edwards, R. L., J. W. Beck, G. S. Burr, D. J. Donahue, J. M. A. Chappell, A. L. Bloom, E. R. M. Druffel, F. W. Taylor, A large drop in atmospheric $^{14}C/^{12}C$ and reduced melting in the Younger Dryas, documented with ^{230}Th ages of corals, *Science, 260*, 962-968, 1993.

Epstein, S., R. Buchsbaum, H. A. Lowenstam, and H. C. Urey, Revised carbonate water isotopic temperature scale, *Geological Society of America Bulletin, 64*, 1315-1326, 1953.

Fairbanks, R. G., The age and origin of the "Younger Dryas Climate Event" in Greenland ice cores, *Paleoceanography, 5*, 937-948, 1990.

Gardner, J. V., W. E. Dean, P. Dartnell, Biogenic sedimentation beneath the California Current system for the past 30 kyr and its paleoceanographic significance, *Paleoceanography, 12*, 207-225, 1997.

Grimm, E. C., G. L. Jacobson, Jr., W. A. Watts, B. C. S. Hansen, and K. A. Maasch, A 50,000-year record of climate oscillations from Florida and its temporal correlation with Heinrich events, *Science, 261*, 198-200, 1993.

BIBLIOGRAPHY (continued)

Grootes, P. M., M. Stuiver, J. W. White, W. C. Johnsen, and J. Jouzel, Comparison of oxygen isotope records from the GISPII and GRIP Greenland ice cores, *Nature, 366*, 552-554, 1993.

Hostetler, S. W., P. U. Clark, P. J. Bartlein, A. C. Mix, and N. G. Pisias, Mechanisms for the global registration of North Atlantic Heinrich Events, *Nature, in press*.

Hutson, W. H., The Agulhas Current during the Late Pleistocene: Analysis of modern faunal analogs, *Science, 207*, 64-66, 1980.

Huyer, A., Coastal upwelling in the California Current System. *Progress in Oceanography, 12*, 259-284, 1983.

Ikeda, M., and W. J. Emery, Satellite observations and modeling of meanders in the California Current System off Oregon and northern California, *Journal of Physical Oceanography, 14*, 1434-1450, 1984.

Imbrie, J., J. D. Hays, D. G. Martinson, A. McIntyre, A. C. Mix, J. J. Morley, N. G. Pisias, W. L. Prell, and N. J. Shackleton, The orbital theory of Pleistocene climate: Support from a revised chronology of the marine record, in *Milankovitch and Climate, Part I*, edited by A. L. Berger, et al., pp. 269-305, D. Reidel Publishing, 1984.

Ingram, B. L., and J. P. Kennett, Radiocarbon chronology and planktonic-benthic foraminiferal ^{14}C age differences in Santa Barbara Basin sediments, Hole 893A in *Proceedings of the Ocean Drilling Program, Scientific Results, Vol. 146*, edited by J. P. Kennett, J. G. Baldauf, and M. Lyle, pp. 19-27, 1995.

Johnsen, S. J., H. B. Clausen, W. Dansgaard, K. Fuhrer, N. Gundestrup, C. U. Hammer, P. Iversen, J. Jouzel, B. Stauffer, and J. P. Steffensen, Irregular glacial interstadials recorded in a new Greenland ice core, *Nature, 359*, 311-313, 1992.

Karlin, R., M. Lyle, and R. Zahn, Carbonate variations in the northeast Pacific during the late Quaternary, *Paleoceanography, 7*, 43-61, 1992.

Keigwin, L. D., and G. A. Jones, Deglacial climatic oscillations in the Gulf of California, *Paleoceanography, 5*, 1009-1023, 1990.

Keigwin, L. D., and G. A. Jones, Western North Atlantic evidence for millennial-scale changes in ocean circulation and climate, *Journal of Geophysical Research, 99*, 12,397-12,410, 1994.

BIBLIOGRAPHY (continued)

Kennett, J. P., and B. L. Ingram, A 20,000-year record of ocean circulation and climate change form the Santa Barbara basin, *Nature, 377*, 510-514, 1995.

Kipp, N. G., New transfer function for estimating past sea-surface conditions from sea-bed distributions of planktonic foraminiferal assemblages in the North Atlantic, in *Investigations of late Quaternary paleoceanography and paleontology*, edited by K. K. Turekian, *Geol. Soc. Am., Mem., 145*, 3-41, 1976.

Kroopnick, P. M., The distribution of ^{13}C of CO_2 in the world oceans, *Deep Sea Research, 32*, 57-84, 1985.

Kutzbach, J. E., Model simulations of the climatic patterns during the deglaciation of North America, in *North America and Adjacent Oceans During the Last Deglaciation, Decade of North American Geology*, edited by W. F. Ruddiman and H. E. Wright, Jr., K-3, 425-447, 1987.

Lehman, S. J., and L. D. Keigwin, Sudden changes in North Atlantic circulation during the last deglaciation, *Nature, 356*, 757-762, 1992.

Lyle, M., R. Zahn, F. Prahl, J. Dymond, R. Collier, N. Pisias, and E. Suess, Paleoproductivity and carbon burial across the California Current: The Multitracers Transect, 42°N, *Paleoceanography, 7*, 251-272, 1992.

Lynch-Stieglitz, J., and R. G. Fairbanks, A conservative tracer for glacial ocean circulation from carbon isotope and palaeo-nutrient measurements in benthic foraminifera, *Nature, 369*, 308-310, 1994.

Mackensen, A., H. Grobe, H. W. Hubberten, and G. Kuhn, Benthic foraminiferal assemblages and the $\delta^{13}C$-signal in the Atlantic sector of the Southern Ocean: glacial-to-interglacial contrasts, in *Carbon Cycling in the Glacial Ocean: Constraints on the Ocean's Role in Global Change*, edited by R. Zahn, T. F. Pedersen, M. A. Kaminski, and L. Labeyrie, pp. 105-144, NATO ASI Series 1, 17, 1994.

Manabe, S., and R. J. Stouffer, Two stable equilibria of a coupled ocean-atmosphere model, *Journal of Climate, 1*, 841-866, 1988.

Mantyla, A. W., and J. L. Reid, Abyssal characteristics of the World Ocean waters, *Deep-Sea Research, 30*, 805-833, 1983.

BIBLIOGRAPHY (continued)

Mantyla, A. W., On the potential temperature in the abyssal Pacific Ocean, *Journal of Marine Research, 33*, 341-354, 1975.

Mikolajewicz, U., T. J. Crowley, A. Schiller, and R. Voss, Modeling teleconnections between the North Atlantic and North Pacific during the Younger Dryas, *Nature, 387*, 384-387, 1997.

Mix, A. C., and N. G. Pisias, Oxygen isotope analyses and deep-sea temperature changes: implications for rates of oceanic mixing, *Nature, 331*, 249-251, 1988.

Ohkouchi, N., H. Kawahata, M. Murayama, M. Okada, T. Nakamura, and A. Taira, Was deep water formed in the North Pacific during the Late Quaternary? Cadmium evidence from the northwest Pacific, *Earth and Planetary Science Letters, 124*, 185-194, 1994.

Oppo, D. W., and S. J. Lehman, Suborbital timescale variability of North Atlantic Deep Water during the past 200,000 years, *Paleoceanography, 10*, 901-910, 1995.

Ortiz, J. D., and A. C. Mix, Comparison of Imbrie-Kipp transfer function and Modern Analog temperature estimates using sediment trap and core top foraminiferal faunas, *Paleoceanography, 12*, 175-190, 1997.

Ortiz, J. D., A. C. Mix, S. Hostetler, and M. Kashgarian, The California Current of the last glacial maximum: Reconstruction at 42°N based on multiple proxies, *Paleoceanography, 12*, 191-205, 1997.

Parker, F., Planktonic foraminiferal species in Pacific sediments, *Micropaleontology, 8*, 219-254, 1962.

Porter, S. C., and A. Zhisheng, Correlation between climate events in the North Atlantic and China during the last glaciation, *Nature, 375*, 305-308, 1995.

Prahl, F. G., N. Pisias, M. A. Sparrow, and A. Sabin, Assessment of sea-surface temperature at 42°N in the California Current over the last 30,000 years, *Paleoceanography, 10*, 763-773, 1995.

Reid, J. L., Jr., *Intermediate waters of the Pacific Ocean*, 85 pp., Johns Hopkins Press, Baltimore, 1965.

BIBLIOGRAPHY (continued)

Sabin, A. L., and N. G. Pisias, Sea surface temperature changes in the Northeast Pacific Ocean during the past 20,000 years and their relationship to climatic change in Northwestern North America, *Quaternary Research, 46*, 48-61, 1996.

Saito, T., P. R. Thompson, and D. Breger, *Systematic index of Recent and Pleistocene planktonic foraminifera*, University of Tokyo Press, Tokyo, Japan, 1981.

Sancetta, C., M. Lyle, L. Heusser, R. Zahn, and J. P. Bradbury, Late-Glacial to Holocene changes in winds, upwelling and seasonal production of the northern California Current System, *Quaternary Research, 38*, 359-370, 1992.

Shackleton, N. J., Carbon-13 in *Uvigerina*: tropical rain forest history and the equatorial Pacific carbonate dissolution cycles, in *The Fate of Fossil Fuel CO_2 in the Oceans*, edited by N. R. Andersen and A. Malahoff, pp. 401-427, 1977.

Shackleton, N. J., J. Imbrie, and M. A. Hall, Oxygen and carbon isotope record of East Pacific core V19-30: implications for the formation of deep water in the late Pleistocene North Atlantic, *Earth and Planetary Science Letters, 65*, 233-244, 1983.

Southon, J. R, D. E. Nelson, and J. S. Vogel, A record of past ocean-atmosphere radiocarbon differences from the northeast Pacific, *Paleoceanography, 5*, 197-206, 1990.

Strub, P. T., P. M. Kosro, A. Huyer, and CTZ Collaborators, The nature of the cold filaments in the California Current System, *Journal of Geophysical Research, 96*, 14743-14768, 1991.

Stuiver, M. and T. F. Braziunas, Modeling atmospheric ^{14}C influences and ^{14}C ages of marine samples to 10,000 BC, *Radiocarbon, 35*, 137-189, 1993.

Sverdrup, H. U., M. W. Johnsen, and R. H. Fleming, *The Oceans*, Prentice-Hall, New Jersey, 1942.

Talley, L. D., An Okhotsk Sea water anomaly: Implications for ventilation in the North Pacific, *Deep-Sea Research, 38*, S171-190, 1991.

Talley, L. D., Distribution and formation of the North Pacific Intermediate Water, *Journal of Physical Oceanography, 23*, 517-537, 1993.

BIBLIOGRAPHY (continued)

Toggweiler, J. R., and B. Samuels, Effect of Drake Passage on the global thermohaline circulation, *Deep-Sea Research*, 42, 477-500, 1995.

van Geen, A., R. G. Fairbanks, P. Dartnell, M. McGann, J. V. Gardner, and M. Kashgarian, Ventilation changes in the northeast Pacific during the last deglaciation, *Paleoceanography, 11*, 519-528, 1996.

Warner, M. J., and G. I. Roden, Chlorofluorocarbon evidence for recent ventilation of the deep Bering Sea, *Nature, 373*, 409-412, 1995.

Warren, B.A., Why is no deep water formed in the North Pacific?, *Journal of Marine Research, 41*, 327-347, 1983.

Zahn, R., K. Winn, and M. Sarnthein, Benthic foraminiferal $\delta^{13}C$ and accumulation rates of organic carbon: *Uvigerina peregrina* group and *Cibicidoides wuellerstorfi*, *Paleoceanography, 1*, 27-42, 1986.

Zahn, R., T. F. Pedersen, B. D. Bornhold, and A. C. Mix, Water mass conversion in the glacial subarctic Pacific (54°N, 148°W): Physical constraints and the benthic-planktonic stable isotope record, *Paleoceanography, 6*, 543-560, 1991.

Appendices

Appendix A

Benthic Foraminiferal Stable Isotopic Data

Depth (cm)	Age (cal ka)*	CIB d18O	CIB d13C	UVI d18O	UVI d13C
40	7.62			3.49	-0.90
60	8.32			3.64	-1.05
80	9.03			3.60	-1.00
99	9.67			3.71	-1.05
102	9.73			3.79	-1.09
105	9.80			3.81	-0.89
108	9.86			3.80	-0.98
112	9.94	3.24	-0.25	3.75	-1.02
115	10.01	3.23	-0.28	3.83	-1.02
118	10.07	3.29	-0.12	3.83	-0.98
121	10.13	3.36	-0.22	3.77	-1.05
124	10.20	3.28	-0.26	3.72	-1.05
127	10.26	3.36	-0.31	3.91	-0.94
130	10.38	3.31	-0.28	3.87	-1.11
133	10.51	3.36	-0.34	3.93	-0.92
136	10.65	3.29	-0.33	3.93	-0.96
139	10.78	3.43	-0.29	4.01	-0.92
142	10.88	3.43	-0.41	3.92	-0.96
145	10.97	3.42	-0.42	3.98	-0.94
148	11.07	3.46	-0.45	4.05	-1.03
151	11.16	3.50	-0.42	4.09	-1.02
154	11.26	3.52	-0.36	4.10	-1.01
157	11.34	3.56	-0.37	4.10	-1.15
160	11.42	3.71	-0.33	4.26	-1.02
163	11.50	3.56	-0.38	4.27	-1.03
166	11.58			4.16	-1.13
169	11.65	3.66	-0.23	4.38	-1.16
172	11.73	3.78	-0.43	4.38	-1.17
175	11.81	3.79	-0.41	4.40	-1.00
178	11.89	3.71	-0.38	4.30	-1.06
181	11.97	3.73	-0.45	4.40	-1.08
184	12.45	3.87	-0.46	4.38	-1.01
187	12.94	3.89	-0.47	4.46	-1.01
190	13.42	3.95	-0.48	4.34	-1.06
193	13.90	3.86	-0.45	4.38	-0.84
196	14.39	3.87	-0.46	4.40	-0.99
199	14.70	3.87	-0.48	4.42	-0.96
202	14.84	3.90	-0.47	4.41	-1.01
205	14.97	3.91	-0.46	4.40	-0.98
211	15.25	4.00	-0.47	4.48	-1.00
214	15.38			4.49	-1.04
217	15.52			4.58	-1.06
221	15.70	3.94	-0.52	4.66	-0.97
224	15.81	4.10	-0.54	4.80	-1.11
227	15.90	4.39	-0.53	4.72	-1.16
230	15.98	4.18	-0.65	4.45	-1.24
234	16.09	4.20	-0.65	4.77	-1.16
237	16.18	4.30	-0.56	4.83	-1.10
239	16.24	4.20	-0.53	4.82	-1.06

Depth (cm)	Age (cal ka)*	CIB d18O	CIB d13C	UVI d18O	UVI d13C
243	16.35	4.26	-0.52	4.82	-1.13
246	16.43	4.30	-0.59	4.85	-1.11
249	16.52	4.27	-0.50	4.91	-1.02
252	16.60	4.33	-0.53	4.91	-1.06
255	16.69	4.40	-0.53	4.68	-1.09
258	16.77	4.36	-0.59	4.87	-1.10
262	16.88	4.30	-0.57	4.87	-1.07
265	16.97	4.30	-0.55	4.98	-1.11
268	17.05	4.34	-0.47	4.97	-1.12
271	17.14	4.31	-0.54	4.95	-1.25
274	17.28	4.29	-0.50	4.95	-1.27
277	17.47	4.32	-0.49	4.98	-1.24
280	17.66	4.41	-0.61	4.97	-1.15
283	17.85	4.34	-0.53	4.98	-1.20
286	18.04	4.36	-0.51		
289	18.24	4.35	-0.52	5.00	-1.23
292	18.43	4.31	-0.47	4.99	-1.22
295	18.62	4.30	-0.51	4.96	-1.14
298	18.81	4.34	-0.43	4.94	-1.14
301	19.00	4.35	-0.53	4.94	-1.26
304	19.19	4.26	-0.49	4.94	-1.13
307	19.37	4.31	-0.55	4.94	-1.21
310	19.55	4.23	-0.57	4.95	-1.19
313	19.73	4.28	-0.47	4.94	-1.15
316	19.91	4.24	-0.59	4.98	-1.23
319	20.09	4.29	-0.54	4.93	-1.20
322	20.27	4.30	-0.53	4.96	-1.17
325	20.45	4.31	-0.57	4.96	-1.17
328	20.63	4.31	-0.49	4.97	-1.21
331	20.81	4.26	-0.47	4.96	-1.18
334	20.99	4.28	-0.50	4.95	-1.18
337	21.17	4.27	-0.53	4.89	-1.20
340	21.34	4.28	-0.56	4.89	-1.14
343	21.52	4.26	-0.53	4.85	-1.06
346	21.70	4.27	-0.50	4.88	-1.18
349	21.87	4.24	-0.54	4.85	-1.21
352	22.05	4.23	-0.56	4.86	-1.16
355	22.23	4.19	-0.56	4.90	-1.22
358	22.40	4.21	-0.49	4.90	-1.11
361	22.58	4.24	-0.49	4.90	-1.17
364	22.76	4.24	-0.56	4.88	-1.12
367	22.94			4.91	-1.16
370	23.11	4.23	-0.50	4.82	-1.13
373	23.29	4.29	-0.49	4.90	-1.11
376	23.47	4.21	-0.44	4.85	-1.17
379	23.64	4.19	-0.44	4.84	-1.19
382	23.82	4.14	-0.48	4.87	-1.11
385	24.00	4.25	-0.46	4.87	-1.11
388	24.17	4.25	-0.37	4.90	-0.93

Depth (cm)	Age (cal ka)*	CIB d18O	CIB d13C	UVI d18O	UVI d13C
391	24.35	4.22	-0.41	4.91	-1.10
394	24.56	4.21	-0.47	4.90	-1.24
397	24.79	4.29	-0.32	4.96	-1.09
400	25.01	4.23	-0.36	4.93	-1.12
403	25.24	4.23	-0.44	5.17	-0.95
406	25.46	4.19	-0.45	5.10	-1.12
409	25.69	4.25	-0.43	5.13	-1.04
412	25.92	4.27	-0.44	5.03	-1.10
416	26.22	4.18	-0.42	4.96	-1.23
419	26.44	4.15	-0.38	4.97	-1.12
422	26.67	4.19	-0.39	4.85	-1.27
425	26.89			4.79	-1.17
428	27.12			4.87	-1.09
431	27.35	4.10	-0.40	4.79	-1.19
434	27.57	4.07	-0.44	4.76	-1.09
437	27.80	4.07	-0.45	4.81	-1.06
440	28.02			4.82	-1.08
443	28.25	4.15	-0.43	4.78	-1.23
446	28.45	4.12	-0.44	4.77	-1.00
449	28.66	4.09	-0.40	4.70	-1.08
452	28.86	4.07	-0.42	4.72	-0.97
455	29.06	4.04	-0.39	4.69	-1.13
458	29.27	4.06	-0.38	4.76	-1.03
461	29.47	4.01	-0.49	4.74	-0.93
464	29.67	4.03	-0.46	4.73	-0.97
467	29.88	4.00	-0.38	4.77	-1.00
470	30.08	4.00	-0.43	4.73	-1.04
473	30.28	4.03	-0.39	4.78	-1.10
476	30.49	4.08	-0.39	4.73	-1.09
479	30.69	4.09	-0.38	4.77	-1.02
482	30.89	4.08	-0.32	4.80	-1.15
485	31.10	4.01	-0.44	4.79	-1.05
488	31.30	4.08	-0.40	4.78	-1.02
491	31.50	4.25	-0.57	4.75	-1.21
494	31.71	4.24	-0.39	4.75	-1.16
497	31.91	4.24	-0.27	4.78	-1.14
501	32.18	4.08	-0.40	4.69	-1.20
504	32.38	4.12	-0.25	4.78	-1.00
507	32.58	4.16	-0.31	4.73	-1.11
510	32.78	3.93	-0.37	4.72	-1.03
512	32.91	3.98	-0.33	4.74	-0.97
514	33.05	4.04	-0.41	4.79	-1.13
517	33.25	4.04	-0.34	4.69	-1.11
520	33.45	4.02	-0.44	4.74	-1.01
523	33.65	3.96	-0.32	4.77	-1.08
526	33.85	3.95	-0.38	4.70	-0.87
529	34.05	4.00	-0.23	4.68	-1.14
532	34.25	3.89	-0.39	4.71	-1.13
535	34.45	3.99	-0.38	4.70	-1.09

Depth (cm)	Age (cal ka)*	CIB d18O	CIB d13C	UVI d18O	UVI d13C
538	34.65	3.98	-0.34	4.68	-1.13
541	34.85	3.93	-0.47	4.74	-1.14
544	35.05	3.85	-0.43	4.71	-0.97
548	35.32	3.85	-0.34	4.78	-1.22
551	35.52	3.94	-0.29	4.80	-1.06
554	35.72	3.84	-0.39	4.74	-1.12
557	35.92	3.81	-0.33	4.69	-1.06
561	36.38	3.92	-0.26	5.18	-0.13
564	36.72	3.93	-0.36		
567	37.06	3.94	-0.44	4.53	-1.16
569	37.29	4.09	-0.21		
572	37.54	3.92	-0.31	4.59	-1.07
575	37.74	3.84	-0.43	4.56	-0.99
578	37.95	3.84	-0.32	4.55	-0.98
581	38.15	3.87	-0.39	4.52	-1.14
584	38.36	3.97	-0.41	4.45	-1.08
587	38.56	3.90	-0.44	4.54	-1.10
590	38.77	3.88	-0.44	4.54	-1.01
593	38.97	3.95	-0.45	4.58	-1.01
596	39.18	3.96	-0.46	4.64	-1.17
599	39.38	3.93	-0.37	4.64	-1.11
602	39.59	3.99	-0.33	4.61	-1.08
605	39.79	4.00	-0.32	4.60	-1.11
608	40.00	4.06	-0.21	4.61	-1.07
611	40.39	4.07	-0.25	4.63	-1.00
614	40.78	4.00	-0.39	4.57	-1.03
617	41.17	3.98	-0.30	4.58	-1.04
620	41.56	4.08	-0.23	4.57	-1.10
623	41.95	3.99	-0.39	4.55	-1.01
626	42.34	4.04	-0.30	4.62	-1.01
629	42.73	4.02	-0.33	4.56	-1.10
632	43.12	3.98	-0.34	4.55	-1.08
635	43.51	4.03	-0.42	4.50	-1.21
638	43.90	3.83	-0.36	4.57	-0.98
641	44.29			4.56	-1.08
644	44.68	3.98	-0.27	4.52	-1.17
647	45.07	3.99	-0.22	4.57	-1.18
650	45.46	3.87	-0.31	4.58	-1.24
653	45.85	3.92	-0.23	4.53	-1.22
656	46.24	3.93	-0.33	4.51	-1.21
658	46.50	3.90	-0.23	4.56	-1.10
662	46.96	3.96	-0.28	4.47	-1.27
665	47.31	3.87	-0.37	4.49	-1.05
668	47.66	3.84	-0.34	4.60	-1.05
671	48.01	3.84	-0.31	4.55	-0.79
674	48.36	3.88	-0.32	4.66	-1.01
677	48.71	3.81	-0.34	4.50	-0.90
680	49.06	3.83	-0.38	4.53	-1.04
683	49.41	3.83	-0.30	4.57	-1.09

Depth (cm)	Age (cal ka)*	CIB d18O	CIB d13C	UVI d18O	UVI d13C
686	49.75	3.91	-0.37	4.58	-1.14
689	50.10	3.94	-0.38	4.63	-1.14
692	50.45	4.02	-0.36	4.66	-1.07
695	50.80	3.92	-0.13	4.63	-1.05
698	51.24	3.85	-0.37	4.55	-1.08
701	51.68	3.94	-0.44	4.62	-0.99
704	52.12	4.01	-0.36	4.66	-1.03
707	52.56	3.93	-0.34	4.61	-1.07
710	53.00	3.88	-0.22	4.60	-1.09
713	53.48	3.87	-0.29	4.56	-1.20
717	54.12	3.69	-0.48	4.52	-1.04
719	54.44	3.86	-0.55	4.48	-1.17
722	54.92	3.81	-0.41	4.53	-1.16
725	55.40	3.80	-0.44	4.46	-1.18
728	55.88	3.79	-0.45	4.49	-1.18
731	56.36	3.89	-0.49	4.47	-1.25
734	56.84	3.87	-0.49	4.65	-1.18
737	57.16	3.76	-0.51	4.58	-1.18
740	57.40	3.91	-0.47	4.60	-1.21
743	57.64	3.89	-0.48	4.63	-1.22
746	57.88	3.86	-0.49	4.61	-1.17
749	58.12	3.85	-0.55	4.56	-1.31
752	58.36	3.84	-0.54	4.61	-1.31
755	58.60	3.78	-0.57	4.55	-1.35
758	58.84	3.68	-0.50	4.47	-1.26
761	59.15	3.85	-0.58	4.47	-1.20
778	61.78	3.80	-0.65		
798	64.87	3.94	-0.63	4.70	-1.35
818	67.96	3.88	-0.68	4.63	-1.17
838	71.05	3.93	-0.54	4.63	-1.32
857	73.99	3.80	-0.40	4.45	-1.25
868	75.69	3.70	-0.31	4.35	-1.15

* Calendar age is based on average age model in Figure 2.1b

CIB = *C. wuellerstorfi*

UVI = *Uvigerina spp.*

d18O= delta oxygen-18

d13C= delta carbon-13

Appendix B

Planktonic Foraminiferal Species Data and Modern Analog Results

Depth (cm)	Age (cal ka)	*%G. bull*	*%G. quin*	*%N. pacL*	*%N. pacR*	*%N. dute*	*%G. scit*	*%G. glut*	*% other*	Coil %	SST, mean	SST, range
99	9.67	9.0	4.5	29.9	46.5	4.5	1.0	4.2	0.3	39.1	11.5	5.8
105	9.80	11.4	7.9	40.1	28.9	7.2	0.6	3.1	0.8	58.1	10.8	5.2
112	9.94	6.5	7.6	18.6	48.6	14.6	0.3	3.8	0.0	27.7	11.3	6.0
118	10.07	7.4	13.1	20.8	34.0	17.0	2.6	4.8	0.3	38.0	11.3	6.0
124	10.20	11.4	14.2	17.2	35.6	14.2	1.4	5.0	1.1	32.6	11.2	6.1
130	10.38	4.5	9.7	29.7	36.1	15.2	0.4	3.3	1.1	45.2	9.0	4.4
136	10.65	2.4	13.0	38.2	33.9	5.8	1.8	4.8	0.0	52.9	7.9	4.1
139	10.78	2.6	12.6	44.7	24.6	6.8	1.3	7.4	0.0	64.5	7.9	4.1
142	10.88	3.7	8.5	59.6	17.0	4.8	0.4	5.2	0.7	77.8	8.4	4.3
145	10.97	1.6	7.6	59.9	15.3	7.3	1.3	7.0	0.0	79.7	8.4	4.3
148	11.07	2.9	6.2	65.5	15.0	5.8	0.0	4.0	0.6	81.4	7.9	4.3
151	11.16	6.3	5.5	61.6	15.9	4.1	0.7	4.4	1.5	79.5	8.7	3.9
154	11.26	3.4	5.9	66.5	10.3	5.6	0.5	7.6	0.2	86.6	7.9	4.3
157	11.34	3.1	7.9	64.8	10.7	4.4	0.9	8.2	0.0	85.8	7.9	4.3
160	11.42	5.0	10.1	55.6	20.1	1.8	0.6	6.5	0.3	73.4	8.2	4.7
163	11.50	4.1	10.5	46.6	24.2	6.8	0.3	6.8	0.7	65.9	7.9	4.1
166	11.58	3.4	21.6	42.4	16.6	4.7	0.7	9.6	0.9	71.8	7.8	4.2
169	11.65	5.7	11.0	42.9	24.7	8.0	0.7	7.0	0.0	63.5	8.7	4.5
172	11.73	6.6	9.6	36.3	29.9	13.2	0.9	3.0	0.4	54.8	9.2	4.1
175	11.81	7.4	8.6	38.0	35.8	6.2	0.3	3.4	0.3	51.5	9.9	4.6
178	11.89	7.6	8.3	39.7	28.8	12.0	0.8	2.3	0.6	57.9	9.2	4.1
181	11.97	12.7	8.6	33.5	31.6	8.9	0.8	2.8	1.1	51.5	11.1	6.0
184	12.45	13.1	10.0	33.4	25.6	10.9	1.6	5.0	0.3	56.6	11.2	6.0
187	12.94	14.7	9.4	37.8	25.5	7.6	0.0	4.1	0.9	59.7	11.1	6.0
190	13.42	15.3	8.2	34.0	19.0	14.2	2.6	5.7	1.1	64.2	11.2	6.0
193	13.90	17.7	8.0	36.7	23.2	5.1	2.3	5.5	1.6	61.3	12.1	6.5
196	14.39	21.1	9.6	33.9	19.3	7.9	0.4	7.1	0.7	63.8	11.1	6.0
199	14.70	27.1	9.4	41.3	7.9	2.0	1.0	10.6	0.8	84.0	10.9	6.2
202	14.84	24.9	8.8	36.3	16.7	7.6	1.4	4.2	0.0	68.5	11.1	6.0
205	14.97	19.9	9.4	39.2	16.8	8.5	0.6	5.1	0.6	70.1	11.2	6.0
211	15.25	30.4	13.0	40.9	4.9	2.6	0.6	7.0	0.6	89.2	9.1	5.6
214	15.38	35.6	9.4	41.2	2.2	2.2	0.5	8.9	0.0	95.0	10.0	6.1
217	15.52	36.6	10.6	37.0	4.0	5.0	0.9	5.6	0.3	90.2	10.3	6.1

Depth (cm)	Age (cal ka)	%G. bull	%G. quin	%N. pacL	%N. pacR	%N. dute	%G. scit	%G. glut	% other	Coil %	SST, mean	SST, range
221	15.70	32.0	7.4	46.3	2.0	3.1	1.1	7.7	0.3	95.9	9.6	6.1
224	15.81	39.7	7.7	42.0	1.7	3.3	0.7	5.0	0.0	96.2	9.8	6.1
227	15.90	43.0	10.6	36.6	2.6	3.4	0.0	3.8	0.0	93.3	9.8	6.1
237	16.18	45.0	2.8	43.5	1.6	3.1	0.9	2.8	0.3	96.6	9.8	6.1
243	16.35	42.5	1.8	48.2	2.0	2.0	0.2	3.3	0.0	96.1	9.7	7.0
249	16.52	36.8	1.8	54.3	1.1	1.6	0.2	3.9	0.2	97.9	9.7	7.0
262	16.88	41.2	3.6	48.1	0.5	1.4	0.5	4.4	0.3	98.9	9.6	6.7
268	17.05	34.1	5.5	53.5	0.7	0.2	0.7	4.9	0.4	98.8	8.5	6.1
274	17.28	40.7	6.0	42.8	1.1	2.5	0.4	6.3	0.4	97.6	9.8	6.1
280	17.66	33.1	5.6	55.6	2.5	0.7	0.4	2.1	0.0	95.8	9.6	6.1
286	18.04	34.3	5.6	52.4	2.8	0.7	0.0	3.5	0.7	94.9	9.6	6.1
292	18.43	32.0	5.0	49.3	4.7	1.4	0.3	7.2	0.3	91.3	10.6	6.3
298	18.81	28.3	6.2	55.3	1.8	0.7	0.7	7.1	0.0	96.9	8.5	6.1

Planktonic foraminiferal species percentages in W8709A-13PC, including depth (±1 cm), age (cal ka), *%G. bull* = *%Globigerina bulloides*, *%G. quin* = *%G. quinqueloba*, *%N. pacL* = *%Neogloboquadrina pachyderma (L)*, *%N. pacR* = *%N. pachyderma (R)*, *%N. dute* = *%N. dutertrei*, *%G. scit* = *%Globorotalia scitula*, *%other*, the coiling percentage of *N. pachyderma* [L/(L+R)]*100, mean modern analog sea-surface temperature (SST) estimate (see text), and estimated SST range. RMS error for mean SST is ±1.5°C [Ortiz *et al.*, 1997].